INTERNATIONAL ATOMIC ENERGY AGENCY
UNITED NATIONS EDUCATIONAL, SCIENTIFIC AND CULTURAL ORGANIZATION

INTERNATIONAL CENTRE FOR THEORETICAL PHYSICS
34100 TRIESTE (ITALY) - P.O.B. 586 - MIRAMARE - STRADA COSTIERA 11 - TELEPHONE: 2240-1
CABLE: CENTRATOM - TELEX 460392-1

SMR/208 - 28

SPRING COLLEGE IN MATERIALS SCIENCE

ON

"METALLIC MATERIALS"

(11 May - 19 June 1987)

DISLOCATIONS
(Part IV)

J.Th.M. DE HOSSON
Department of Applied Physics
University of Groningen
9747 AG Groningen
The Netherlands

OUTLINE: "DISLOCATIONS" - SPRING COLLEGE MAI

1 DEFECTS IN CRYSTALS

2 OBSERVATION OF DISLOCATIONS

3 MOVEMENT OF DISLOCATIONS

4 PLASTIC PROPERTIES OF DISLOCATIONS

5= DISLOCATIONS IN FACE-CENTRED CUBIC MET

6 DISLOCATIONS IN OTHER CRYSTAL STRUCTURES

- HEXAGONAL CLOSE-PACKED METALS
- BODY-CENTRED CUBIC METALS
- DISLOCATIONS IN SUPERLATTICES
- DISLOCATIONS IN COVALENT CRYSTALS
- DISLOCATIONS IN IONIC CRYSTALS
- DISLOCATIONS IN POLYMER CRYSTALS

7- DISLOCATION DYNAMICS

- NUCLEAR SPIN-RELAXATION THEORY ADAPTED FOR DISLOCATION MOTION
- SPIN RELAXATION DUE TO DISLOCATION MOTIO
- MOVING DISLOCATIONS IN IONIC MATERIA
- MOVING DISLOCATIONS IN METALS
- MOVING DISLOCATIONS IN ALLOYS.

simple cubic

STACKING SEQUENCE (100) planes : A A A A

(110) planes : A B A B

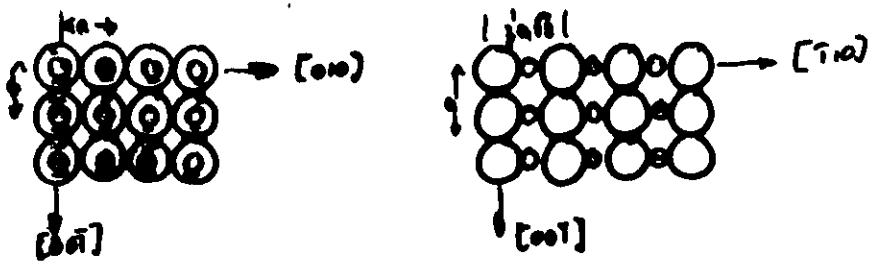

body-centred cubic

stacking sequence {100} {110} : A B A B A B

{112} planes: A B C B E F A B C

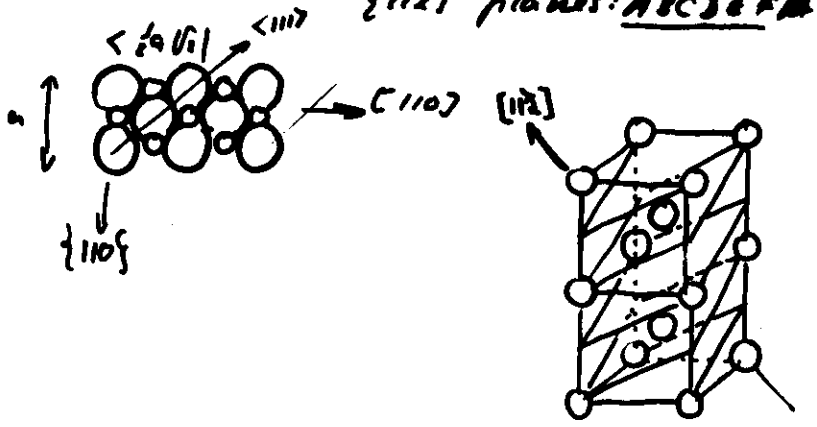

face - centred cubic

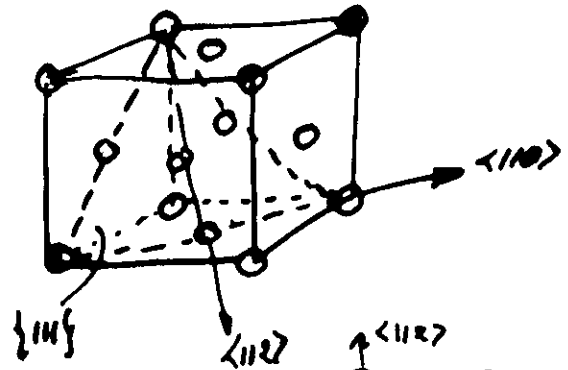

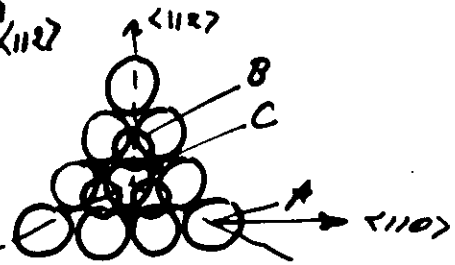

{111} : ABC A BC ...

hexagonal close packed:

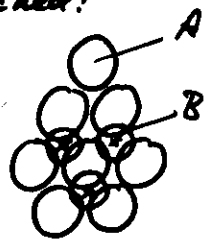

{0001} : ABABAB

FRANK PARTIAL: $\frac{1}{3}\langle 111\rangle$

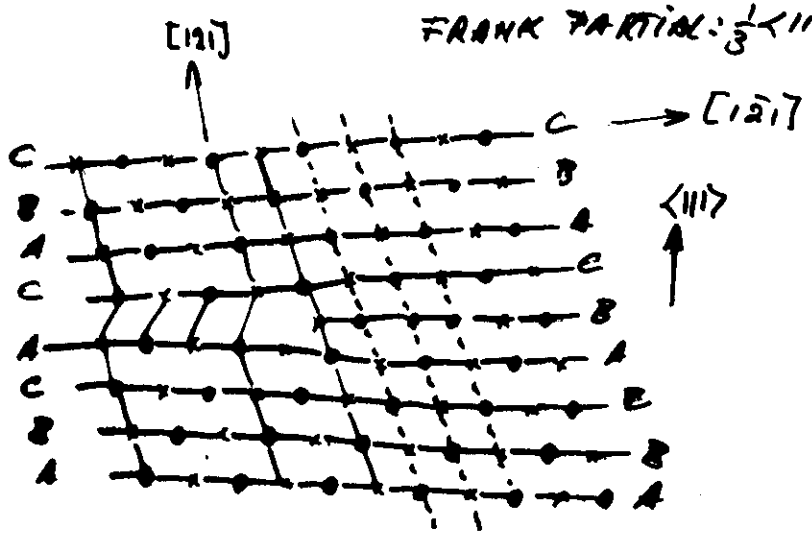

SHOCKLEY PARTIAL $\frac{1}{6}\langle 112\rangle$

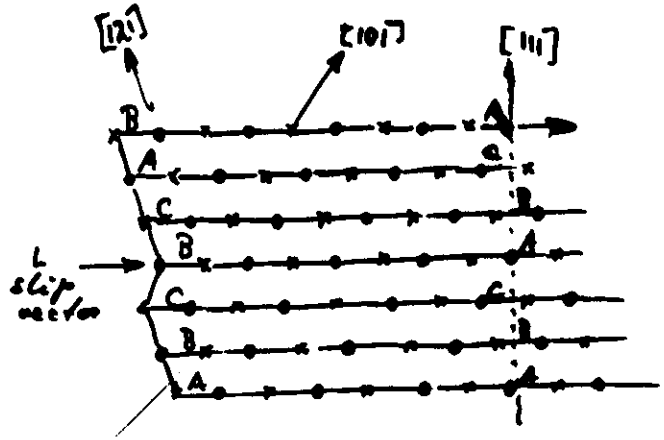

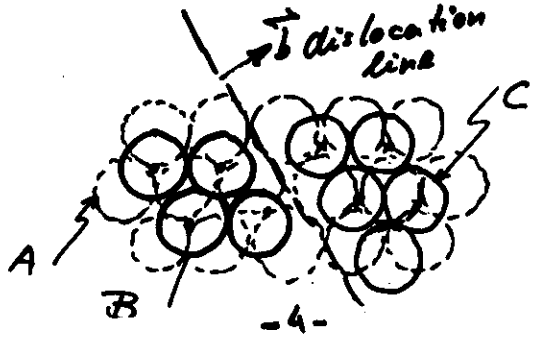

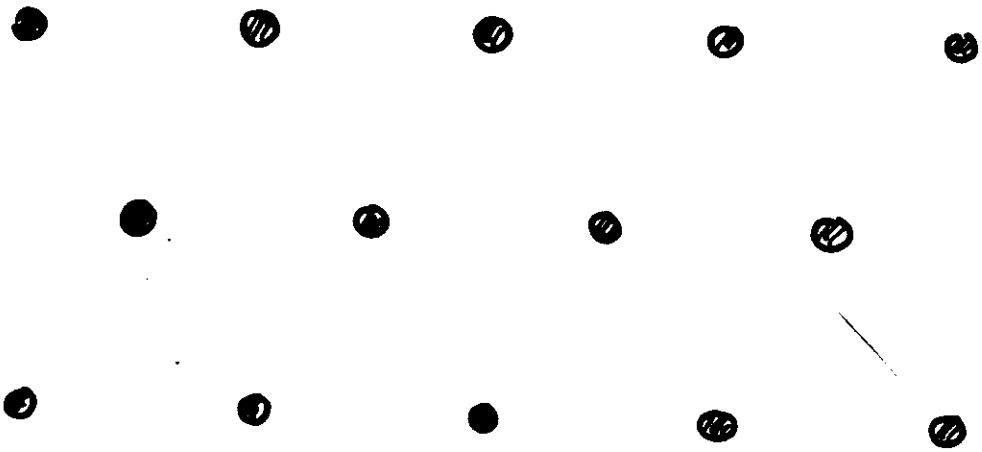

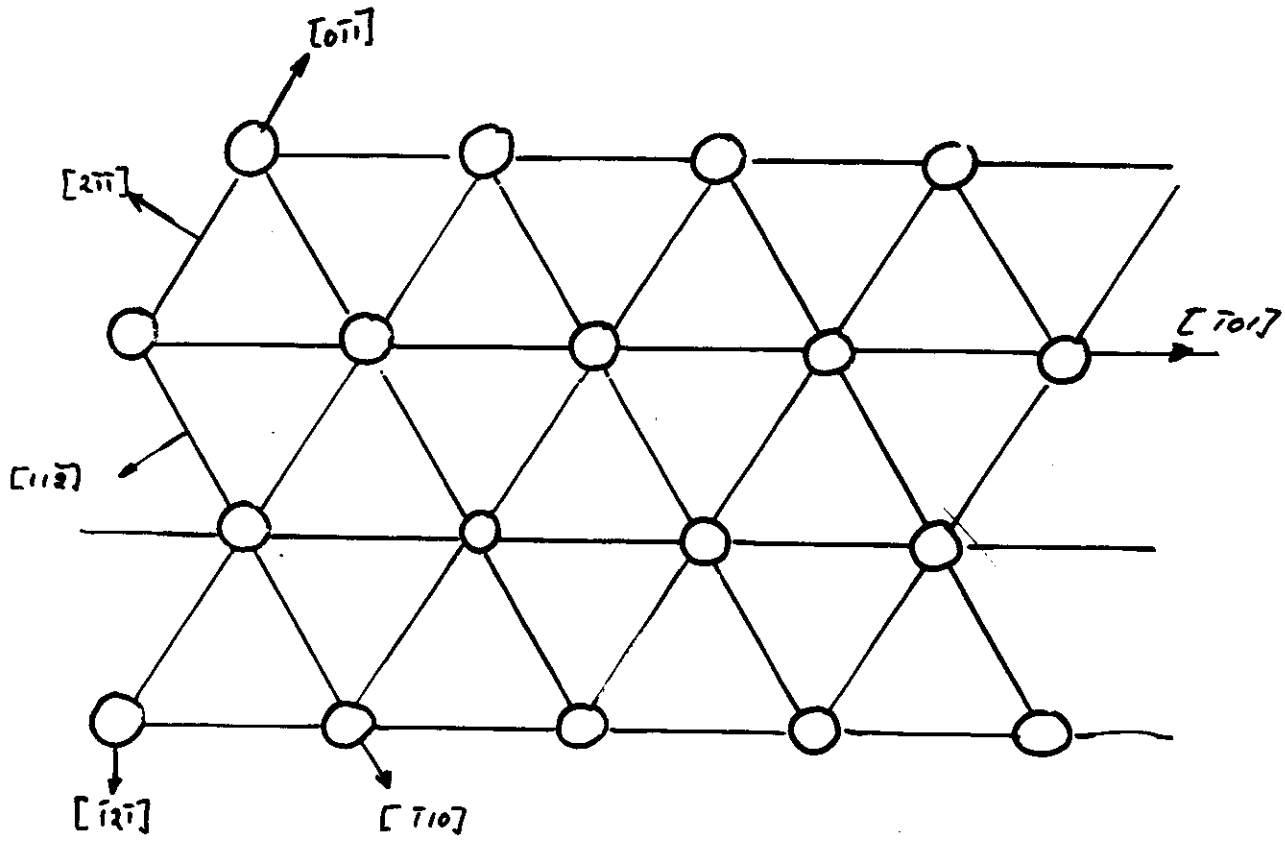
[0$\bar{1}$1]
[2$\bar{1}$1]
[$\bar{1}$01]
[11$\bar{2}$]
[$\bar{1}$2$\bar{1}$]
[$\bar{1}$10]

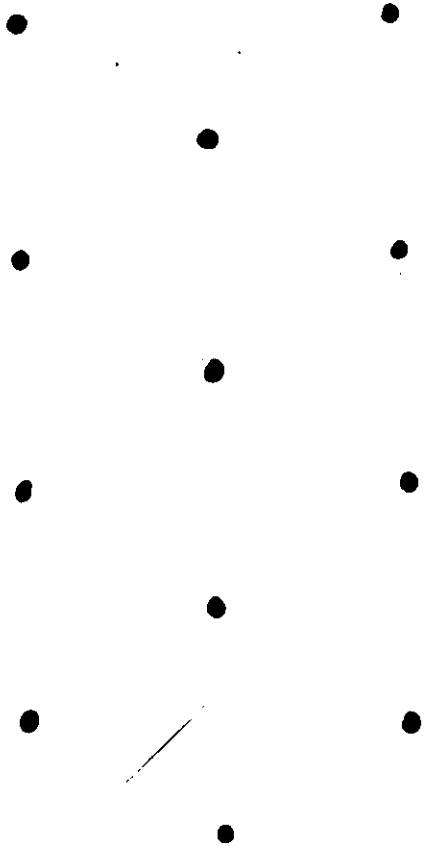

SHEAR LOOP

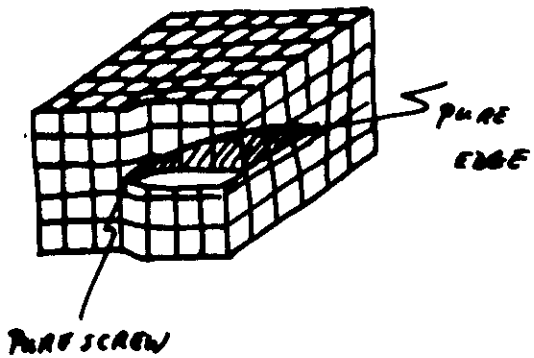

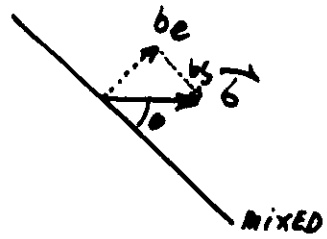

$\vec{b}_F = \frac{1}{3}[111]$

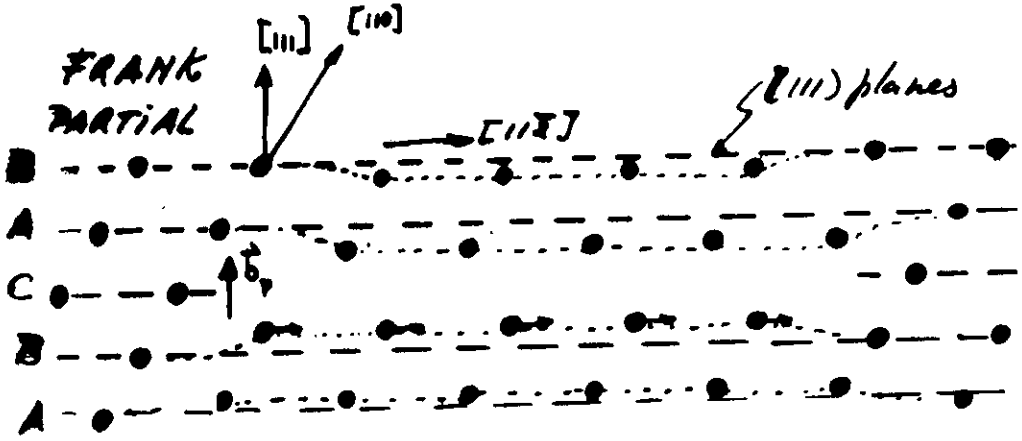

APPLY $b_{SHOCKLEY} = \frac{1}{2}[11\bar{2}]$

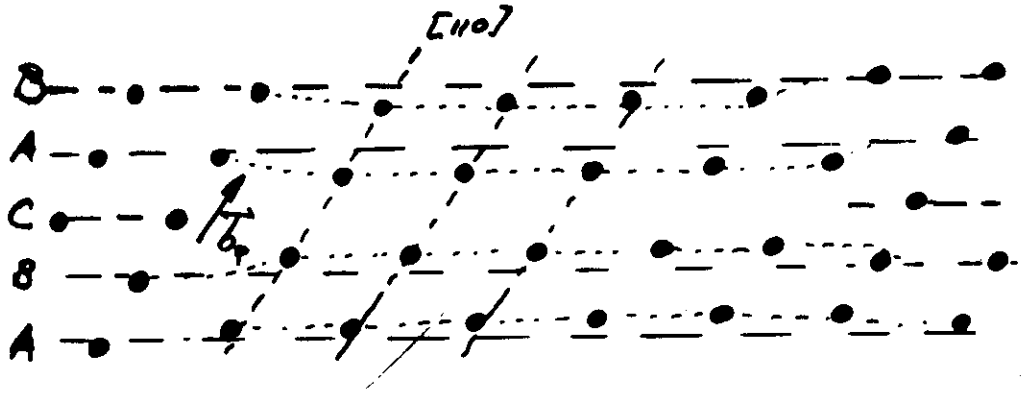

$$\frac{1}{3}[111] + \frac{1}{6}[11\bar{2}] \longrightarrow \frac{1}{2}[110]$$

PERFECT LOOP

on (111)

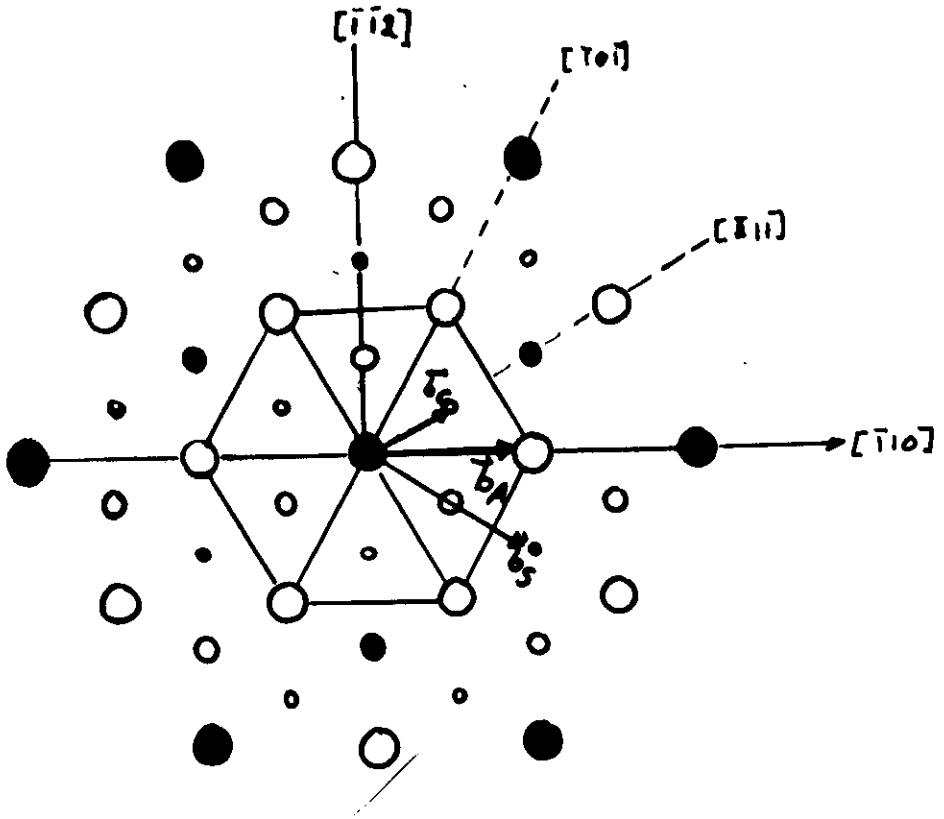

$\vec{b}_A : \frac{1}{2}[\bar{1}10]$ APB — ANTI PHASE BOUNDARY

$\vec{b}_C : \frac{1}{6}[\bar{2}11]$ CSF — COMPLEX STACKING FAULT

$\vec{b}_S : \frac{1}{3}[\bar{1}2\bar{1}]$ SISF — SUPER LATTICE INTRINSIC STACKING FAULT

A_3B

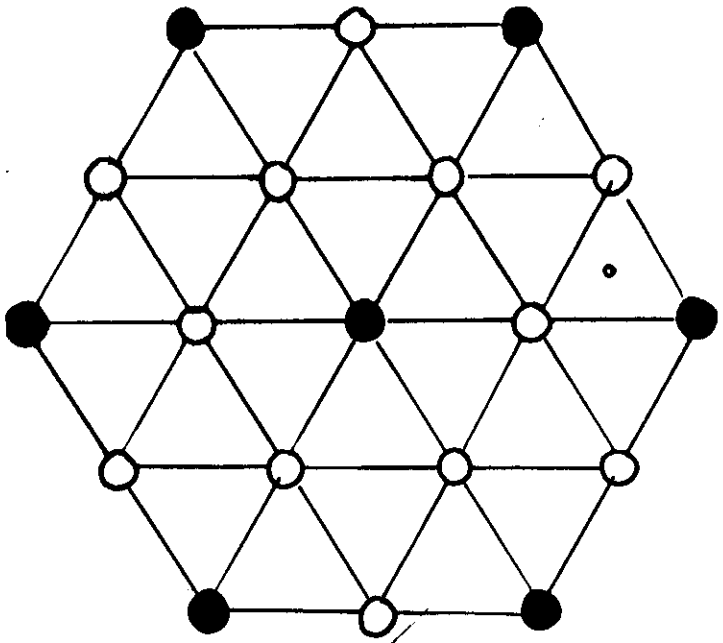

SUPER LATTICE DISLOCATIONS IN $L1_2$

on (111)

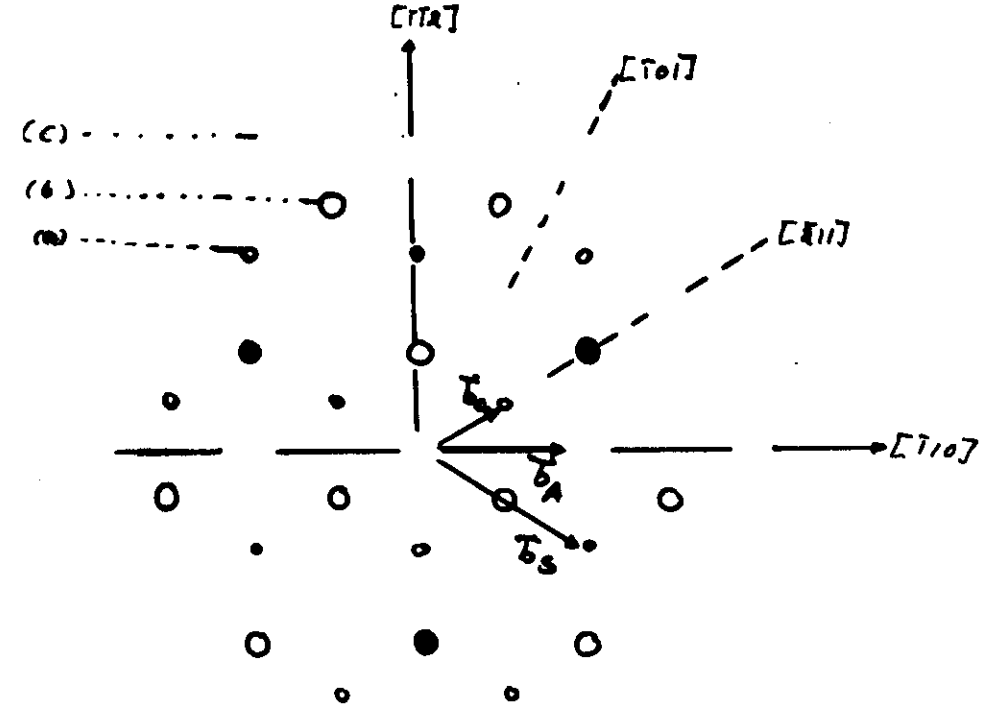

$\vec{b}_A : \frac{1}{2}[\bar{1}10]$ APB ANTI PHASE BOUNDARY

$\vec{b}_C : \frac{1}{6}[\bar{2}11]$ CSF COMPLEX STACKING FAULT

$\vec{b}_S : \frac{1}{3}[\bar{1}2\bar{1}]$ SISF SUPER LATTICE INTRINSIC STACKING FAULT

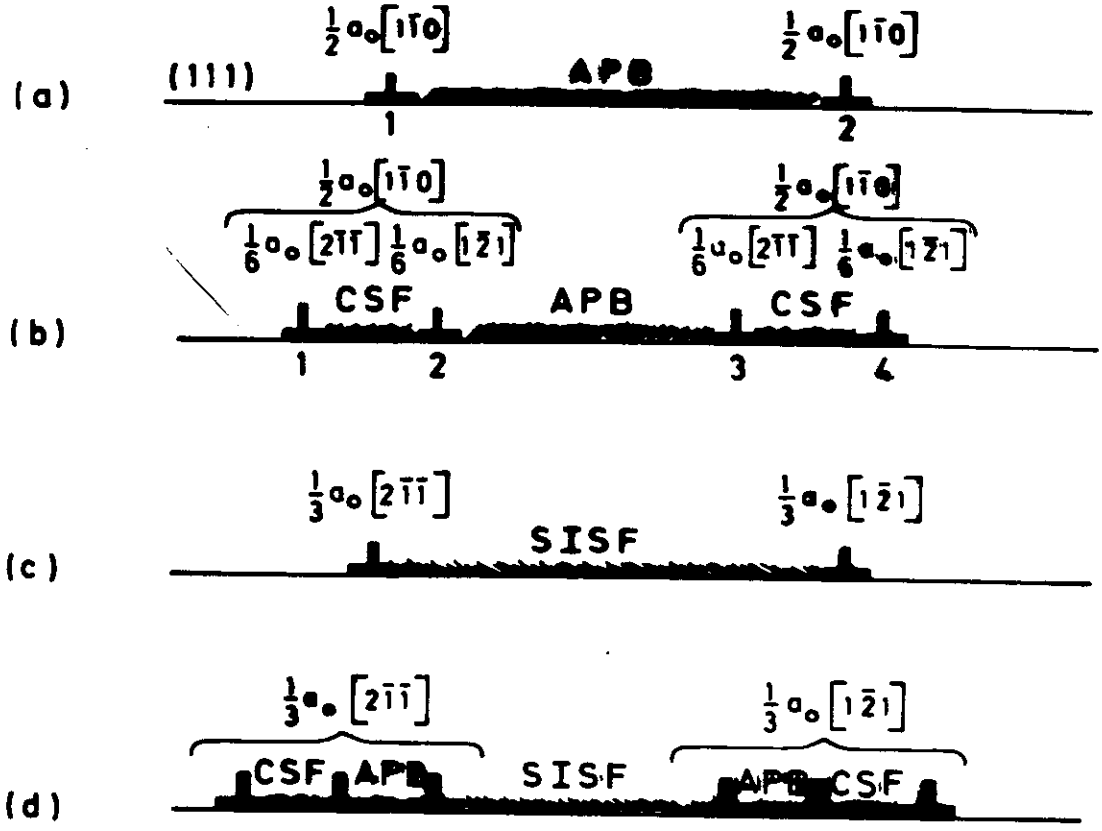
(a)
(111)
$\frac{1}{2}a_0[1\bar{1}0]$
APB
$\frac{1}{2}a_0[1\bar{1}0]$
1
2
(b)
$\frac{1}{2}a_0[1\bar{1}0]$
$\frac{1}{6}a_0[2\bar{1}\bar{1}]$ $\frac{1}{6}a_0[\bar{1}21]$
CSF
APB
CSF
1
2
3
4
(c)
$\frac{1}{3}a_0[2\bar{1}\bar{1}]$
SISF
$\frac{1}{3}a_0[1\bar{2}1]$
(d)
$\frac{1}{3}a_0[2\bar{1}\bar{1}]$
CSF
APB
SISF
APB
CSF
$\frac{1}{3}a_0[1\bar{2}1]$

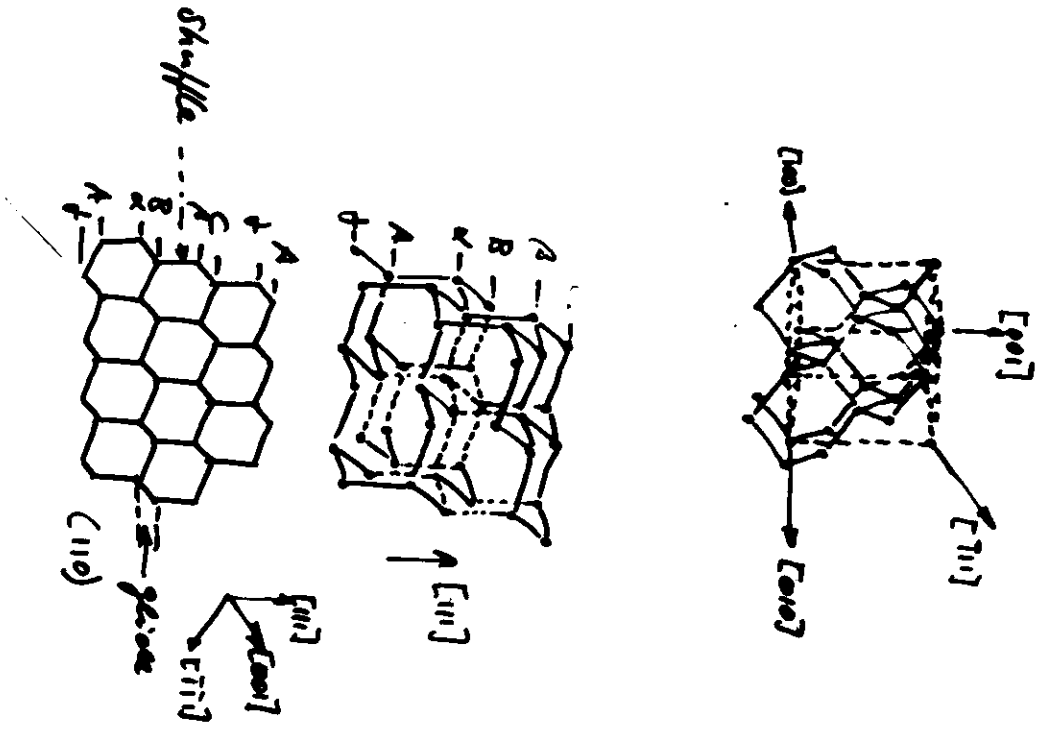
Shuffle
(110)
[111]
[001]
[110]
[111]

number of unpaired electrons

$n = 2 \sin\Theta / \sqrt{3}\, b$ [cm^{-1}]

60° dislocation in the diamond structure

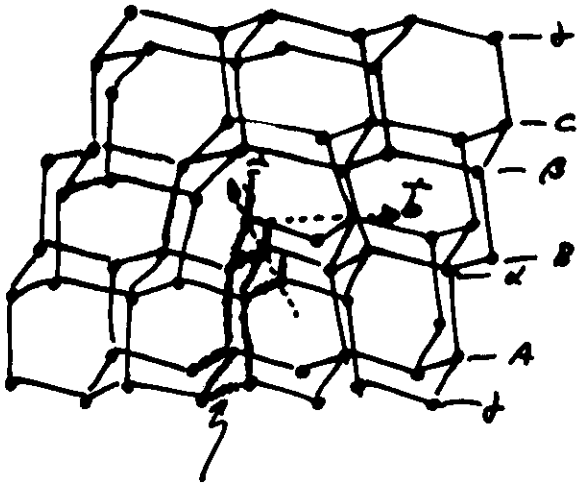

extra half plane

$\vec{\xi}$: dislocation line

$\vec{b}$: Burgers vector

Polymers

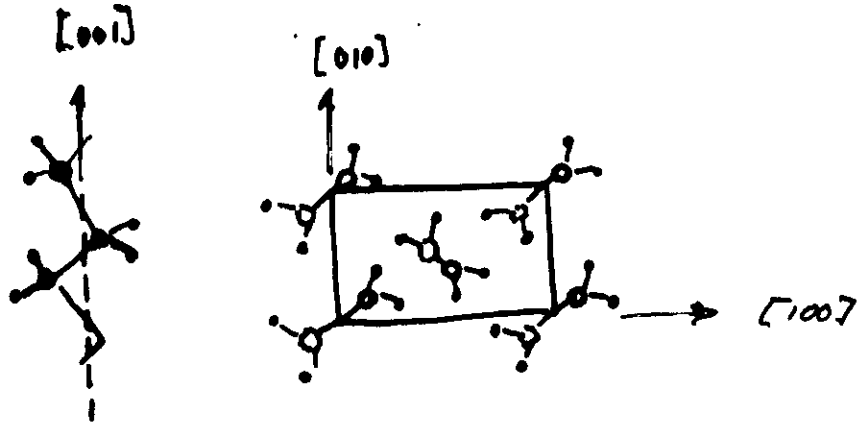

orthorhombic phase

Dislocation glide on {100}{110}

AFTER

1934

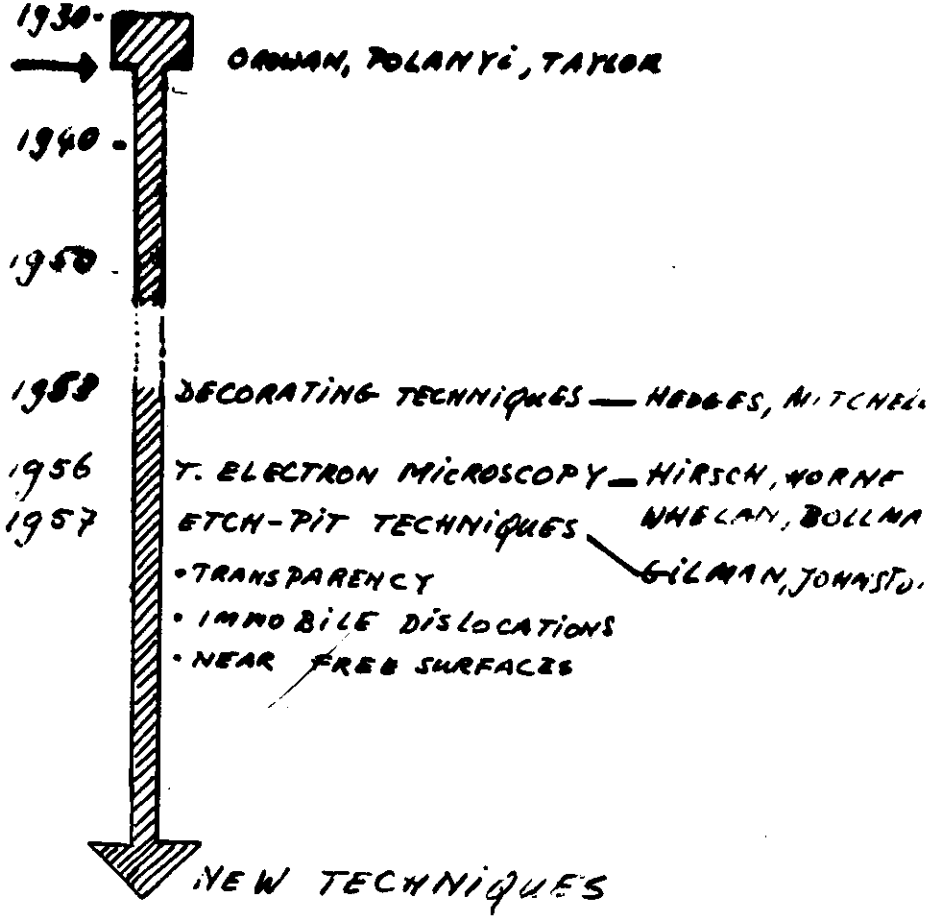

UN. OF GRONINGEN
The Netherlands

TEM

UN. OF DORTMUND
FRG, O. Kanert

NMR

DISLOCATION DYNAMICS INVESTIGATED BY MEANS OF NMR/TEM

The great strength of NMR is:

(i) resonance signal is characteristic of the particular nucleus being studied

$$\omega_0 = \gamma_N H_0 \qquad \mu_N = \gamma_N \hbar I$$

(ii) resonance frequency, linewidth, relaxation time are affected by "surroundings"

NMR applied to constant shear rate experiments which are governed by Orowan's equation:

$$\dot{\varepsilon} = b \rho_m \frac{L}{\tau_N}$$

NMR ⟷ DISLOCATIONS

line broadening, R_2 spin lattice relaxation $R_1 = 1/T_1$

METHOD IS ESSENTIALLY BASED ON the INTERACTION BETWEEN:

ELECTRIC FIELD GRADIENTS AT THE NUCLEUS $\left(\frac{\partial^2 V}{\partial x_i \partial x_j}\right)_k$ ⟸ NUCLEAR ELECTRIC QUADRUPOLE MOMENT $\left(\hat{Q}_{ij}\right)_k$

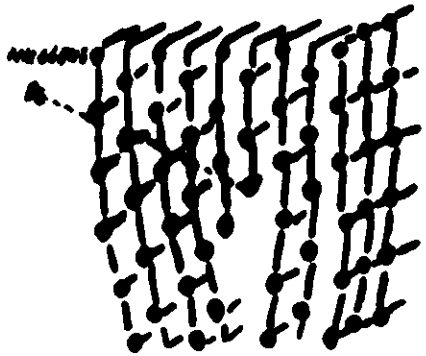

DISTURBED CUBIC SYMMETRY

$$\frac{\partial^2 V}{\partial x_i \partial x_j} \neq 0$$

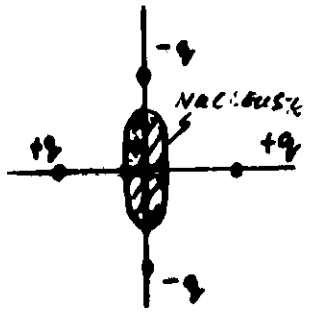

ELECTROSTATIC ENERGY DEPENDS ON ORIENTATION OF THE NUCLEUS

$\hat{Q} \neq 0 \quad (I > \frac{1}{2})$

EXTRA TERM IN THE INTERACTION HAMILTONIAN

$$\hat{\mathcal{H}} = \hat{\mathcal{H}}_Z + \hat{\mathcal{H}}_D + \hat{\mathcal{H}}_Q \longrightarrow \sum_k^{N_k} \sum_{i,j}^{3} \left(\hat{Q}_{ij} \frac{\partial^2 V}{\partial x_i \partial x_j}\right)_k$$

Quadrupole frequency shift $\omega_Q(\sigma)$ vs σ_0

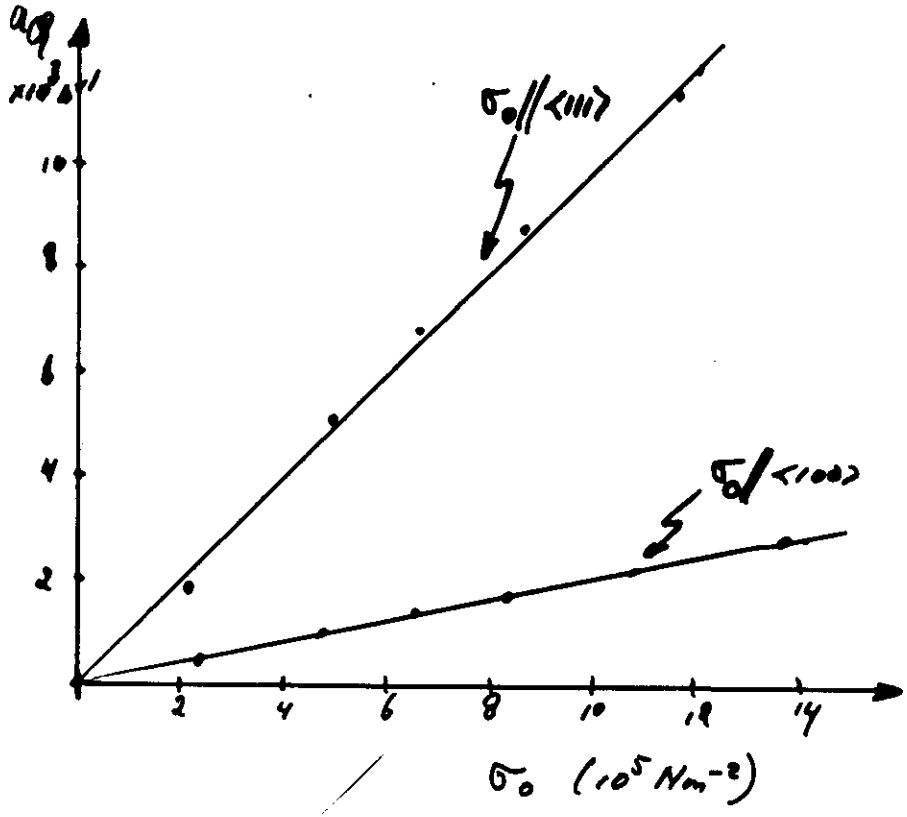

Die Abbildung 5.10 zeigt exemplarisch ein Kernspin-Echo von ^{27}Al:1.6at%Mg.

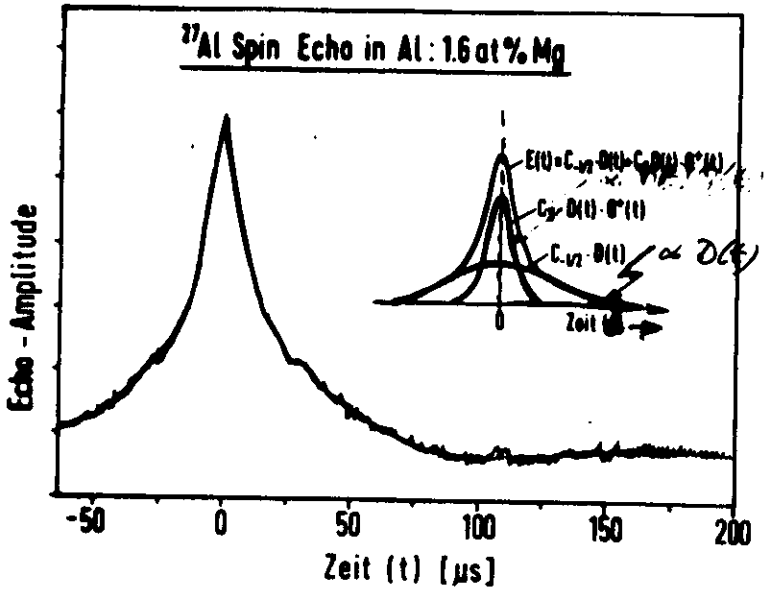

Abb. 5.10 : Kernspin-Echo von ^{27}Al in Al:1.6 at% Mg, T=77 K.
Probe wurde bis zum Riß verformt, I = 5/2
$C_{-1/2}$ = 0.247, $C_g \cdot Q^*(t)$ = 0.468 Q(2t) + 0.285 Q(4t)

Bei der Bestimmung der Lokalfelder wurde deren Spannungsabhängigkeit, bzw. Verformungsabhängigkeit nicht berücksichtigt. Unmittelbar nach Beendigung der NMR-Verformungsexperimente wurden jeweils Quadrupol-Echo-Signale aufgenommen und aus deren Linienform die Lokalfelder bestimmt. Die in der nachfolgenden Tabelle 5.2 aufgeführten Werte für B_L stellen jeweils Mittelwerte über mehrere Proben dar.

Tabelle 5.2

Lokalfelder B_L der untersuchten Proben-Sorten

Legierung	B_L [mT]
Al (5N)	0.316
Al: 8.6 at% Li (215°C)	0.375
Al: 8.6 at% Li (245°C)	0.375
Al: 1.0 at% Zn	0.350
Al: 1.5 at% Zn	0.378
Al: 2.0 at% Zn	0.418
Al: 1.6 at% Mg	0.702
Al: 0.2 at% Mg	0.336
Al: 0.6 at% Mg : 1.0 at% Zn	0.477
Al: 1.2at% Mg : 2.5 at% Zn	0.764

page.
26 Lecture note.
III

SPIN-LATTICE RELAXATION T_1 / $T_{1\rho}$

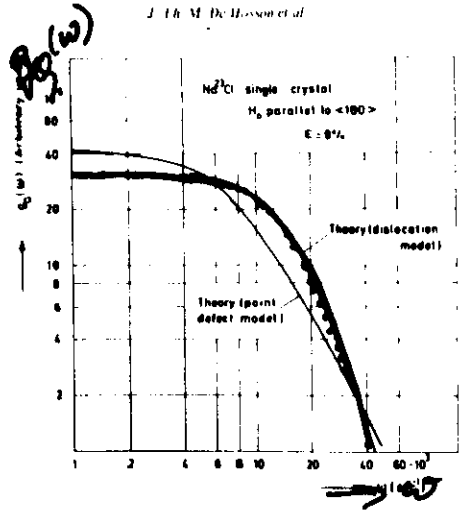

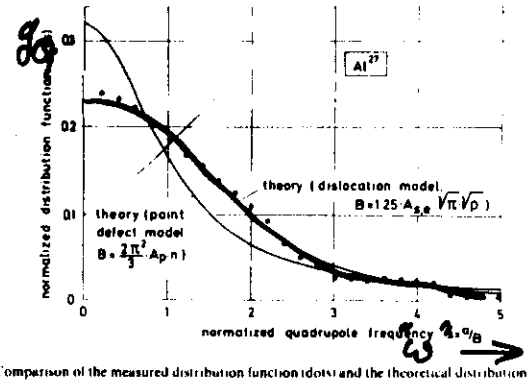

Fig. 14. Comparison of the measured distribution function (dots) and the theoretical distribution function $g_0(\omega)$ for dislocations and for point defects (spin $I = \frac{1}{2}$). The experimental values are obtained from NMR wide-line signals by a numerical deconvolution procedure. (a) deformed ^{23}NaCl single crystal and (b) deformed Al crystal [103].

ion ^{27}Al in aluminum
broadening mechanism
demonstrate clearly th
experimental data, in
defects.

3.4. Effect of dislocatio

In ultra-pure crystals,
this case, the resulting
the total density ρ, of
half width $a_{1/2}$, the ab
moment $\langle a^2 \rangle^{1/2}$ of the
In all the cases the br
the square root of the t

$$\langle \omega_0^2 \rangle = A\rho,$$

with $A = \gamma\pi^2 A_{5,6}^2 \langle b_{\perp}^2 \rangle$
discussion, one has to t
locations are different
abundances of screw to
system of the lattice, the

$$\langle \omega_0^2 \rangle = \gamma\pi^2 \left(A_5^2 \sum_i \right.$$

From the orientation de
of $\langle \omega_0^2 \rangle$ is expected in ge
different planes can be n

4 Nuclear spin relaxat

4.1. Motion-induced spin

While static quadrupolar
tions are analyzed in ter
dynamical effects origina
the motion of defects, suc
deformation, are studied
Following the sudden
diamagnetic sample, the
mon-spin degrees of freed
nuclear magnetization M

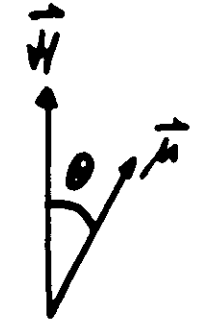

classical equation of motion of a magnetic moment $\vec{\mu}$ in $\vec{H}$ field:

$$\left.\frac{d\vec{\mu}}{dt}\right|_{Lab} = \vec{\mu} \times \gamma \vec{H}$$

$\vec{\mu}$ precesses around $\vec{H}$ with an angular frequency ω:

$$\frac{d\vec{\mu}}{dt} = \frac{\delta\vec{\mu}}{\delta t} + \vec{\omega} \times \vec{\mu} = \vec{\mu} \times \gamma \vec{H}$$

$$\left.\frac{\delta\vec{\mu}}{\delta t}\right|_{\rho} = \vec{\mu} \times (\gamma \vec{H} + \vec{\omega})$$

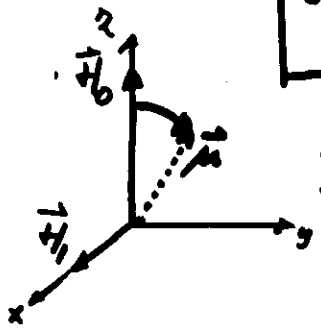

$$\vec{H} = \vec{H}_0 + \frac{\vec{\omega}}{\gamma} + \vec{H}_1$$

SPIN-LATTICE RELAXATION
"L" , "τ_M" , "T_{1M}"

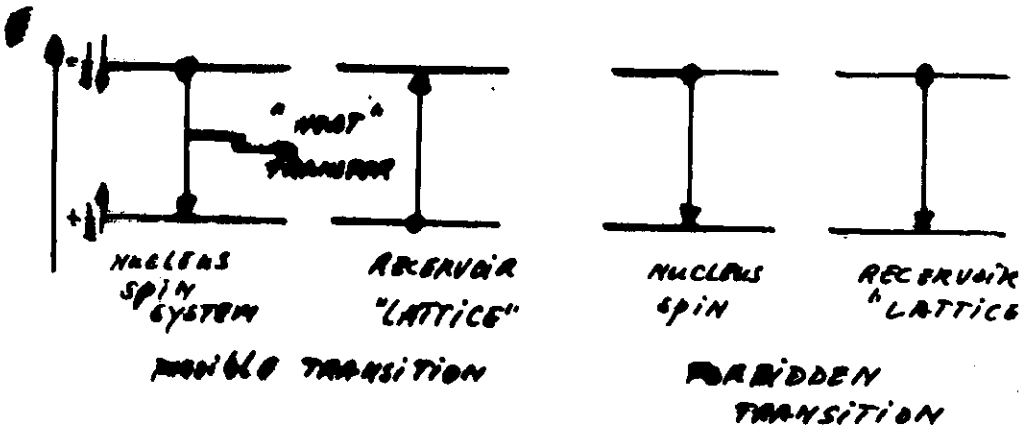

RELAXATION OF $\vec{M}(t)$ to EQUILIBRIUM

T_1 characterizes the time needed to magnetize an unmagnetized sample

$$\frac{d}{dt}\vec{M}(t) = -\frac{1}{T_1}\left[\vec{M}(t) - \vec{M}_0\right]$$

$$M_{\text{Field direction}} = M_0\left(1 - e^{-\frac{t}{T_1}}\right)$$

Fluctuations (in time) in the lattice can introduce energy transfer, i.e. relaxation rate of the magnetization towards equilibrium can be enhanced

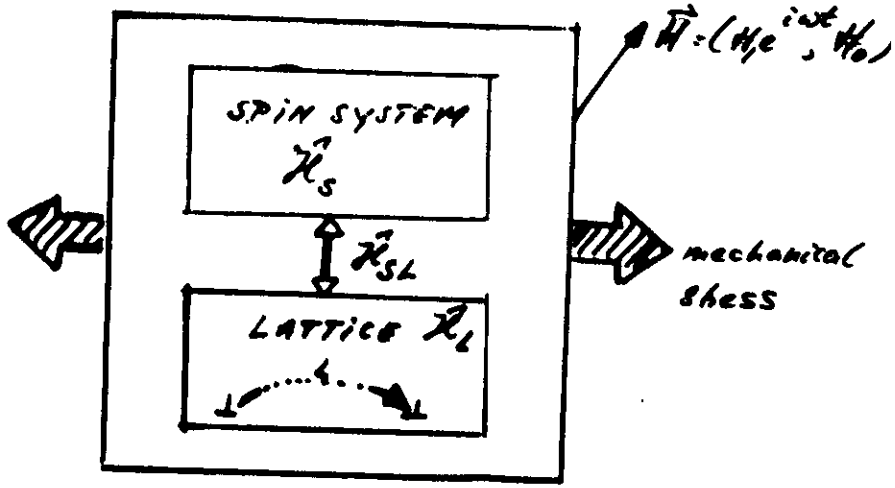

τ_c >> T_m

quadrupolar lattice correlation time (mean time between changes in EFG)

Thermal mixing of spins following a dislocation jump

$$\left.\frac{1}{T_{1P}}\right|_{Dis} \propto \beta(H_1, H_{loc}, \rho_m)\,\frac{1}{\tau_c}$$

$$\left.\frac{1}{T_{1P}}\right|_{Dis} \propto \alpha(H_1, H_{loc})\,\frac{\dot{\varepsilon}}{bL}$$

} $\dot{\varepsilon}$ exc b_i

$$\hat{H} = \hat{H}_S + \hat{H}_L + \hat{H}_{SL}(t)$$

"Golden rule"

$$\frac{1}{T_1} = \frac{2}{\hbar^2} \mathrm{Re} \int_0^\infty dt' \langle a | H_{SL}^*(t') | b \rangle \langle b | H_{SL}^*(0) | a \rangle$$

(average spin-ensemble)

$\hat{H}_{SL}$ = lattice function × spin-operator

semiclassical:

classical → $G(t) = \frac{1}{N} \sum \langle F_{jk}(t') F_{jk}^*(t+t') \rangle_{t'}$

quantum mech. → $f(I)$

(time average)

assume: (Bloembergen)

$$G(t) = \langle F(0)^2 \rangle e^{-\frac{t}{\tau_{NMR}}}$$

τ_{NMR} : mean time between two consecutive changes in EFG

: NMR correlation time

at resonance:

$$\frac{1}{T_1} \simeq \frac{3}{} \langle \omega_{SL}^2(0) \rangle \frac{\tau_{NMR}}{1 + \omega_0^2 \tau_{NMR}^2}$$

strength of coupling SC

Fig. 16

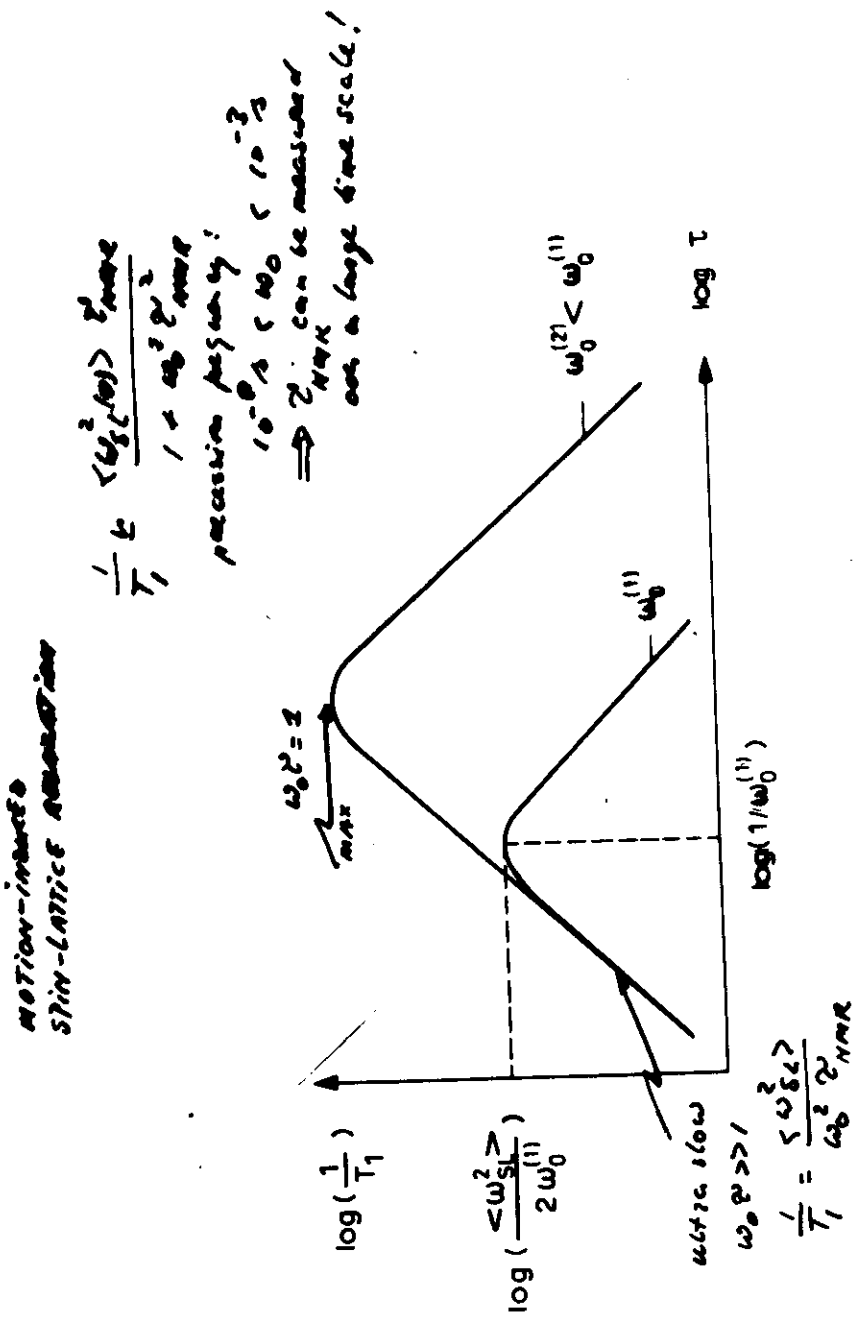

Dislocation motion

$\frac{1}{T_1}$ at maximum if $\frac{1}{\tau_{NMR}} \simeq \omega$

($H_0 = 1.4\ T$, $\omega_0 = 15.8\ M$

Dislocation motion:

$$\frac{1}{\tau_{NMR}} \ll \gamma H_0 \quad \left(\frac{1}{\tau_c} \simeq 10^4\ Hz \right)$$

As a result:

a reduce $\vec{H}_0$ (loss of sensitivity)

b work in the 'rotating frame' at resonance

$$\gamma \vec{H}_{eff} = \gamma \vec{H}_0 + \vec{\omega} + \gamma \vec{H}_1$$

at resonance

$$\gamma \vec{H}_0 + \vec{\omega} = 0$$

→ "$T_{1\rho}$" $\quad \gamma \vec{H}_{eff} = \gamma \vec{H}_1$ (small r.f.)

Thermally activated jerky motion

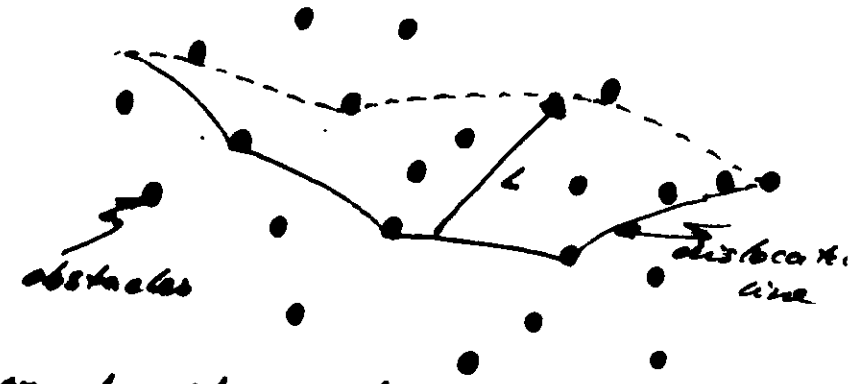

Mean shear strain rate

$$\dot{\varepsilon} = \phi\, b\, \rho_m\, \bar{v}$$

ϕ : Taupin factor

ρ_m = mobile dislocation density

$\bar{v}$ = mean velocity

$$\bar{v} = \frac{L}{\tau_m} = \frac{L}{\tau_w}$$

τ_m is $\tau_{waiting} = \tau_{correlation}^{NMR}$

$$\frac{1}{T_1} \propto \langle \omega_{el}^2(0) \rangle \frac{\tau_{NMR}}{1+\omega_0^2 \tau_{NMR}^2}$$

↓

STRONG COLLISION AT RESONANCE

$\omega_0 \rightarrow \omega_{H} \rightarrow \omega_1 + \omega_0 + \omega_\varphi$

ω_1 RF; $\omega_0 + \omega_\varphi$: Local fields $\gg W_L$

↓

$$\frac{1}{T_{1\rho}} \propto \frac{H_\varphi^2 \frac{\rho_m}{\rho_L} \tau_{NMR}}{1 + (H_1^2 + H_{Loc}^2)\tau_{NMR}^2}$$

with slow motion:

$$\frac{1}{T_{1\rho}} \propto \frac{H_\varphi^2 \frac{\rho_m}{\rho_L}}{(H_1^2 + H_{Loc}^2)\tau_{NMR}} \qquad \dot{\varepsilon} = \phi \rho_m \frac{L}{\tau_N}$$

↓

$$\frac{1}{T_{1\rho}} = \frac{A_\varphi}{H_1^2 + H_{Loc}^2} \cdot \frac{1}{\phi} \frac{\dot{\varepsilon}}{L}$$

Experimental set-up

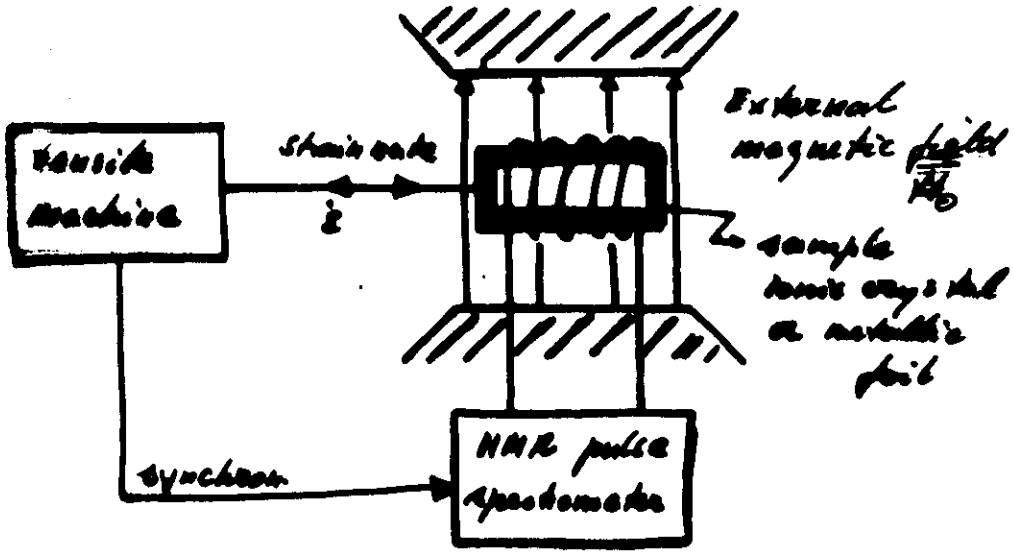

$$\left.\frac{1}{T_{1\rho}}\right|_{dial} = \left.\frac{1}{T_{1\rho}}\right|_{\dot{\varepsilon}\neq 0} - \left.\frac{1}{T_{1\rho}}\right|_{\dot{\varepsilon}=0}$$

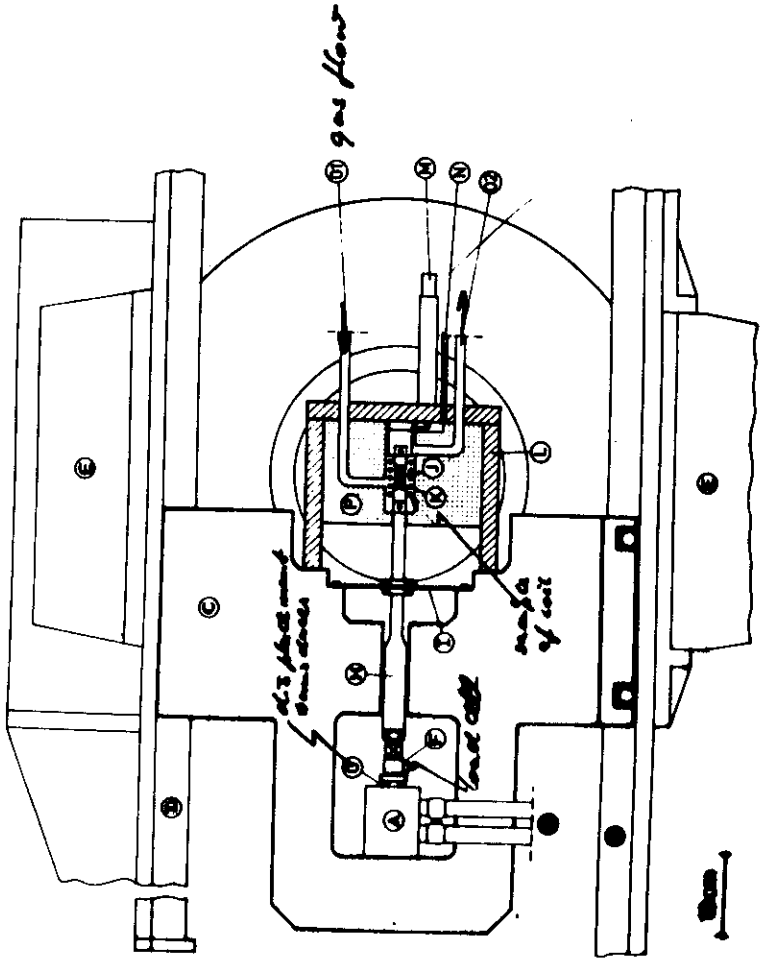

RSI/MAR 83/m-3/fig. 3/f: 55 %

FIG. 3 of 6
Hackel Beer
R&S

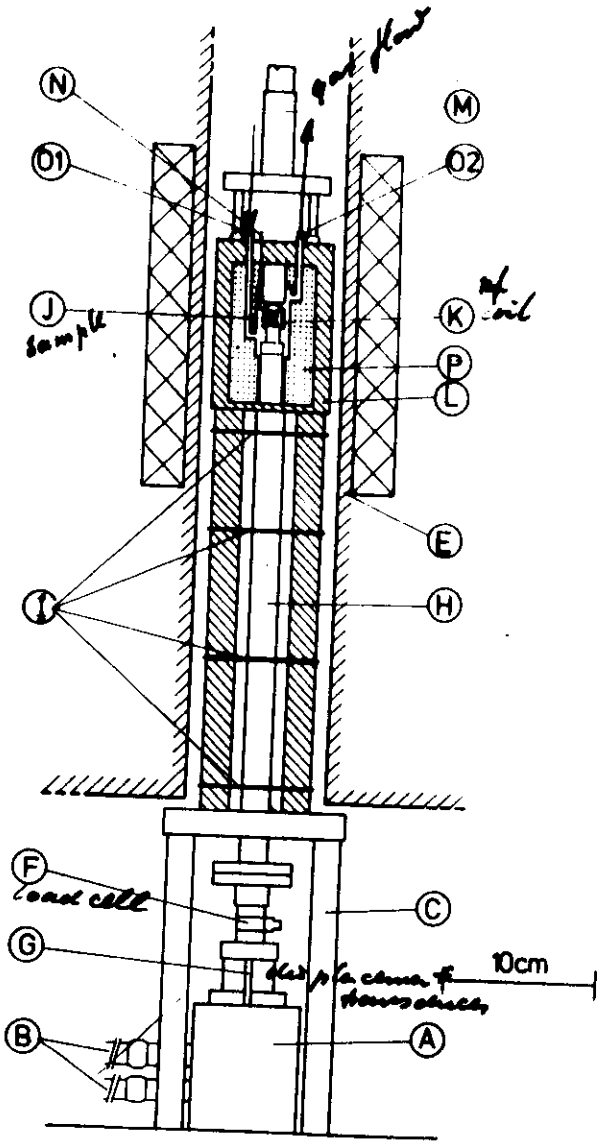

RSI/MAR 83/m-3/fig.4/f: 60 %

for superconducting magnet
(viola bore 8.8 cm)

FIG. 4 of 6
Hackel Beer
R&E

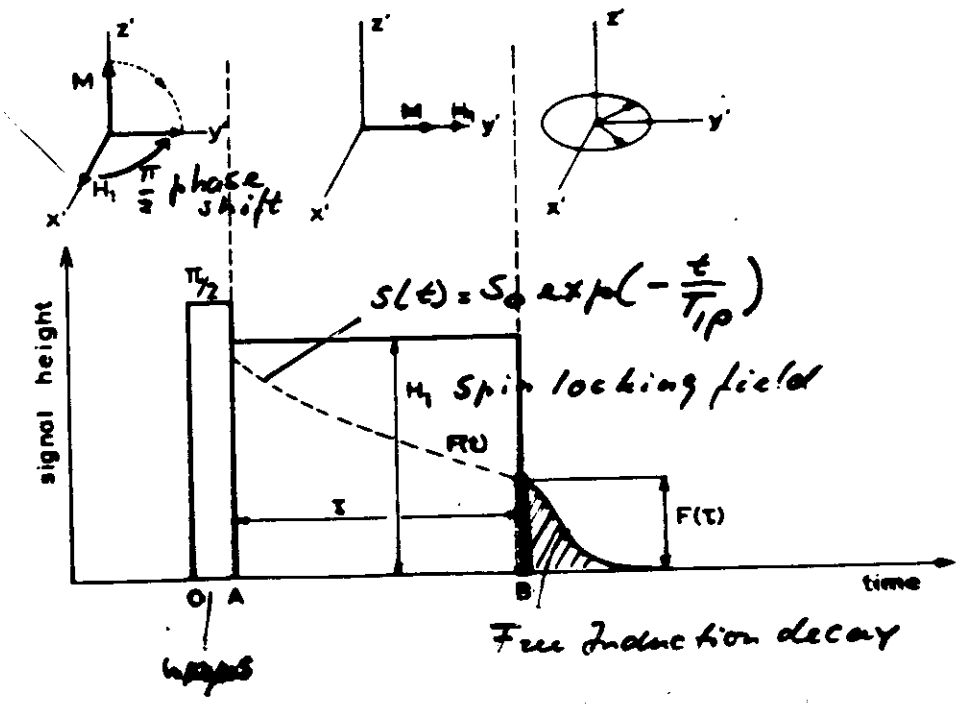

$$\frac{1}{T_{1\rho}}\Big|_0 = \frac{1}{T_{1\rho}}\Big|_{\dot\varepsilon\neq 0} - \frac{1}{T_{1\rho}}\Big|_{\dot\varepsilon=0} = \frac{1}{\tau_L}\ln\frac{F(\tau_L,\dot\varepsilon\neq 0)}{F(\tau_L,\dot\varepsilon=0)}$$

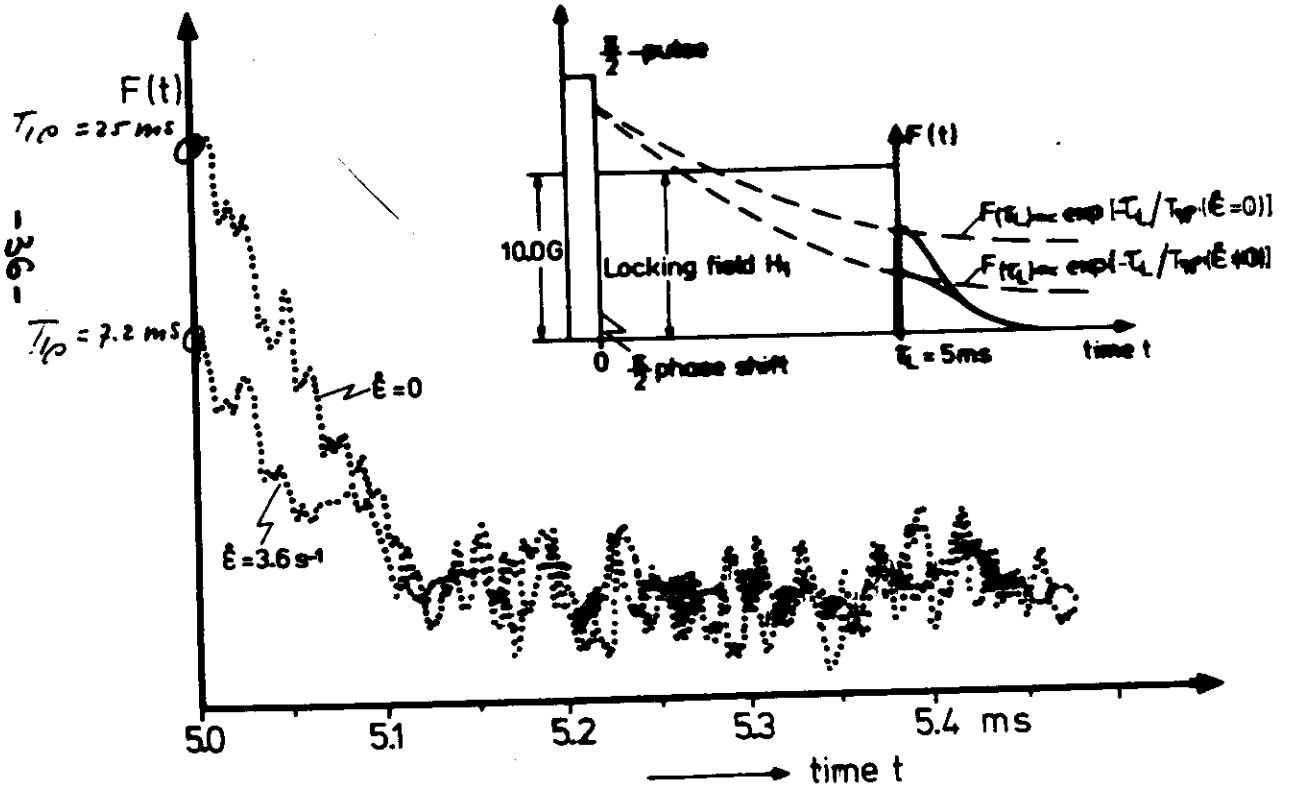

$$\frac{1}{T_{1\rho}} = \frac{H_1^2 \frac{\tau_m}{\tau_N} \tau_{max}}{1 + H_{eff}^2 \tau_{max}^2}$$

$$\dot{\varepsilon} = \delta \frac{\tau_m}{\tau_N} \qquad (\tau_c = \tau_{max})$$

$$H_{eff}^2 \tau_{max}^2 \gg 1$$

$$\frac{1}{T_{1\rho}} = \frac{A(\dot{\varepsilon})}{H_1^2 + H_{Loc}^2} \frac{1}{\delta^2} \dot{\varepsilon}^2$$

$$\frac{1}{T_{1\rho}} \text{ vs } \dot{\varepsilon}$$

p. 55

5.1.3. *Mechanical tester*

In fig. 21 the part of the assembly between the pole pieces of the magnet is shown schematically [84]. The inner rod (brass) can be displaced relative to the outer ones with a constant velocity. The distance between the rods was fixed by diaphragms with a large stiffness perpendicular to the axis of the rods and a low stiffness in the displacement direction. The diaphragms prevented the bars from buckling: this was effective up to a load of 200 kgf, and the maximum load in the experiments did not exceed this value. The cross-head templates were manufactured from polyvinyl chloride, so as to avoid bringing metal into the coil during a test. The cross-head velocity could be varied from 10^{-5} s^{-1} to 10 s^{-1}. No plastic deformation took place in the machine itself. The direction of compressive deformation always lies perpendicular to the external field H_0.

The stress was measured by a strain-gauge load cell and the elongation by an inductive displacement transducer. Measurements at temperatures lower than room temperature were carried out by using a hollow polyvinyl chloride cylinder around the coil as a cryostat and blowing N_2 vapour through it. Temperature stability of about ± 1°C, which could be sensitively determined by the variation of the pressure, was usually reached in about half an hour.

The part of the tensile machine shown was placed in the gap of a 10 in. Bruker BE-25 magnet with a current stabilizer and an external Bruker NMR stabilizer B-SN 15.

An overview of the experimental set-up is depicted schematically in fig. 22. Detailed information can be found in [217].

and the probe head. D is ...plexen, P are the PVC ...on rod [145].

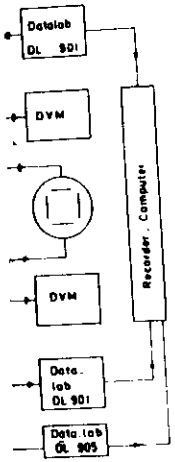

5.2. Measurements of T_1, $T_{1\rho}$ and T_2 during plastic deformation of ionic crystals

The first investigation concerned the existence of the effect of a finite plastic deformation rate on the zero-field spin relaxation time ($H_1 = 0$). Using the Jeener pulse sequence [156], signals for two states $\dot{\varepsilon} \neq 0$ and $\dot{\varepsilon} = 0$ were compared for the three single crystals with three different resonant nuclei: the results are presented in fig. 23.

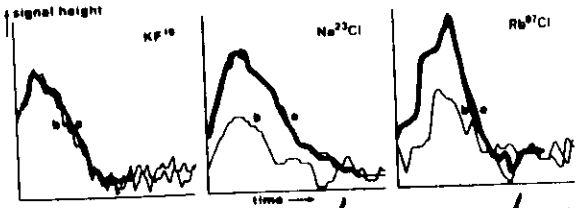

Fig. 23. Signal after a $(\frac{1}{2}\pi - T_2 - \frac{1}{6}\pi; \frac{1}{3}\pi - \tau - \frac{1}{6}\pi)$ pulse sequence as a function of time. The signal height is proportional to $\exp(-\tau/T_{1\rho})$ [159]. $K^{19}F$: a. $\dot{\varepsilon} = 0$; b. $\dot{\varepsilon} = 3 \times 10^{-4}$ s^{-1}; a. $T_{1\rho} = 30$ s; b. $T_{1\rho} = 30$ s; $T = +20$ °C, $\tau = 4$ s, $R_0 = 0$. $^{23}NaCl$: a. $\dot{\varepsilon} = 0$; b. $\dot{\varepsilon} = 3.3 \times 10^{-4}$ s^{-1}; a. $T_{1\rho} = 4.7$ s; b. $T_{1\rho} = 2.1$ s; $T = +20$ °C, $\tau = 3.5$ s, $R_0 = 0.26$ s. $Rb^{87}Cl$: a. $\dot{\varepsilon} = 0$; b. $\dot{\varepsilon} = 1.9 \times 10^{-4}$ s^{-1}; a. $T_{1\rho} = 1.45$ s; b. $T_{1\rho} = 0.49$ s; $T = -196$ °C, $\tau = 3.5$ s, $R_0 = 0.26$ s.

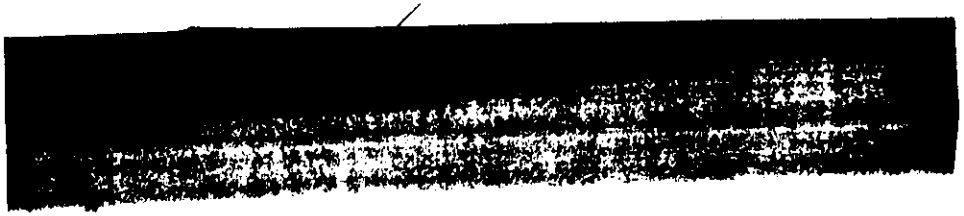

p. 60.
Lecture notes.

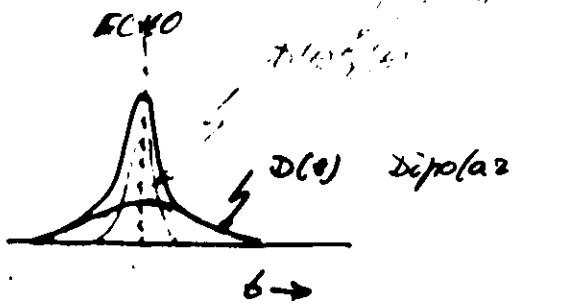

ECHO : $E(t) = C_1 D(t) + C_2 D(t) g(\epsilon)$

$g(\epsilon) \longrightarrow g_{eff}(\omega) \longrightarrow \langle \omega_\phi^2 \rangle = C_3 C_{elec}$

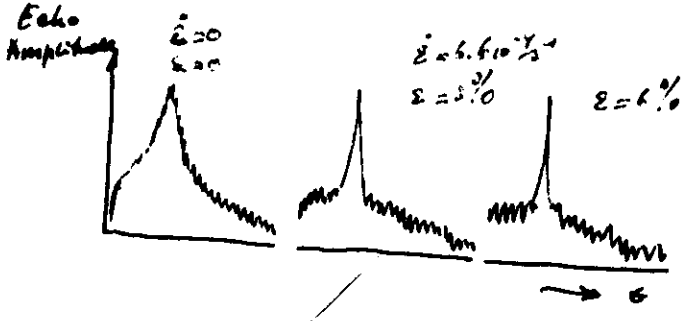

15 a

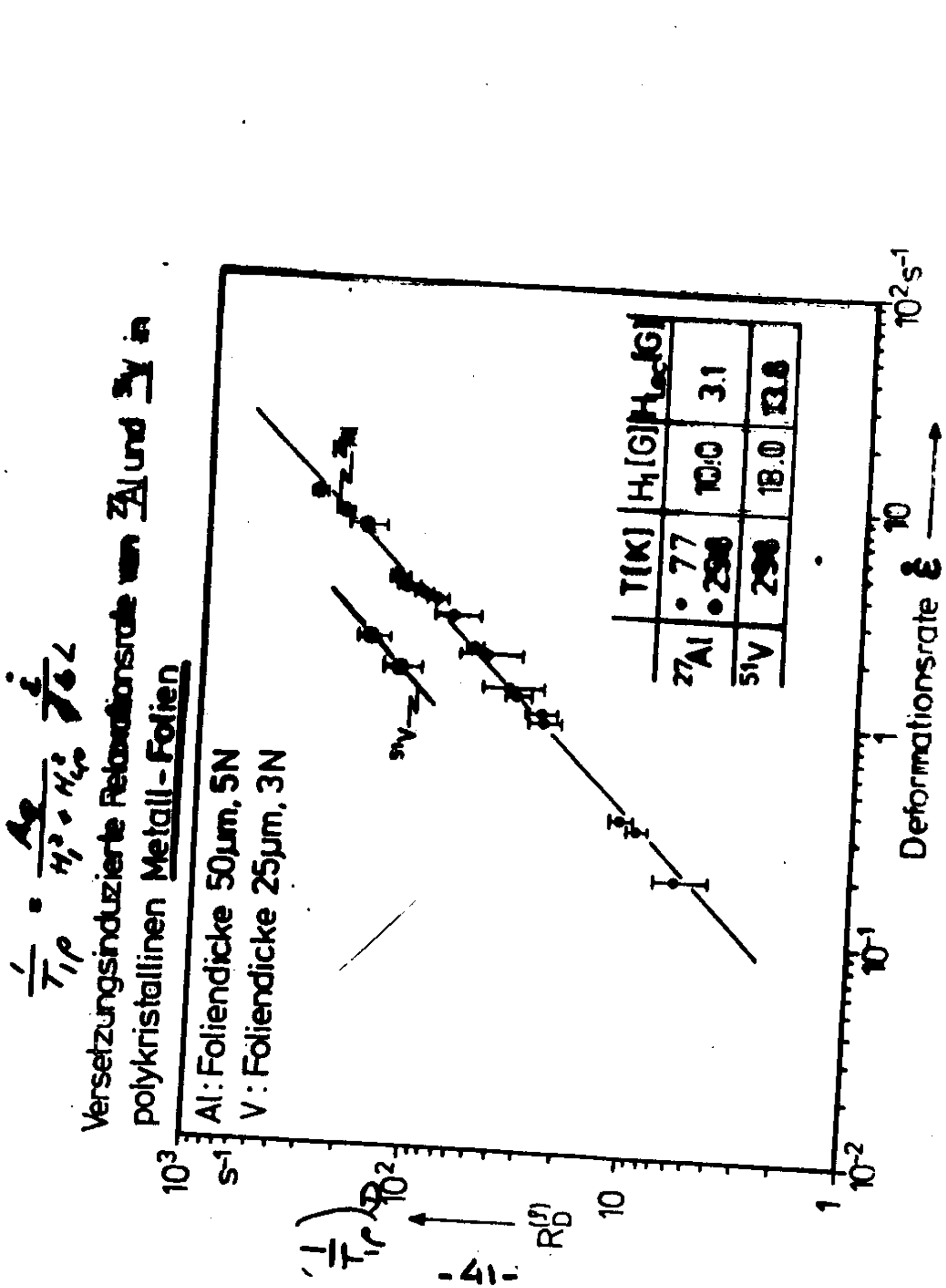

p. 62.

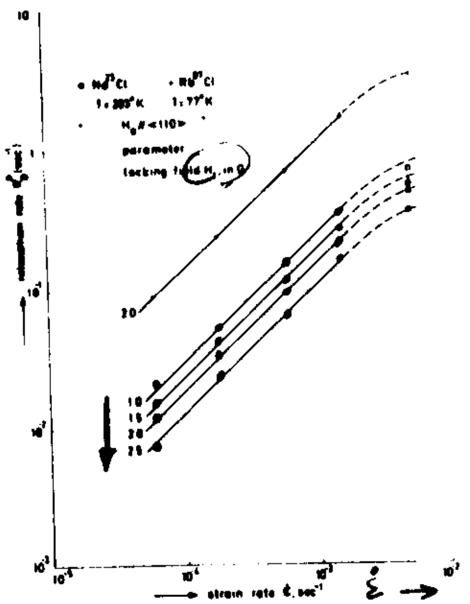

Fig. 31. Experimental data of R^{ρ}_{D} for ^{23}Na and ^{87}Rb as functions of $\dot{\varepsilon}$ [84].

relative to H_0. No orientation dependence was observed within an error of about 10%; this is in good agreement with the theoretical model used for the calculation of $g_Q(L)$ as described earlier in sect. 4.

So far only the qualitative agreement between theory and experiment has been discussed. In order to determine whether there is a quantitative agreement the values of the different parameters of eq. (129), viz. $\delta_Q\langle V^2\rangle$, $\langle\omega_D^2\rangle$ and $\langle\omega_Q^2\rangle$ should be known.

For the shape of the free induction decay after the locking pulse (see fig. 27) the following expression holds ([103], p. 10):

$$F_a(t) = c_{-1/2}D(t) + c_s D(t)Q^+(t), \tag{131}$$

where $F_a(t)$ is the normalized decay function, $c_{-1/2}$ and c_s are the transition probability coefficients and $D(t)$ and $Q^+(t)$ the dipolar and quadrupolar Fourier cosine transforms, respectively, of the distribution functions.

With $I = \frac{3}{2}$ for ^{23}NaCl one obtains ([103], pp. 62ff):

$$c_{-1/2} = 0.4, \qquad c_s = 0.6, \qquad Q^+(t) = Q(2t). \tag{132}$$

Fig. 32. $T_{1\rho D}$ of

Assuming C

$D(t) = e$

and

$Q(t) = ($

where (Δ^2)
and $\frac{1}{2}(\omega_Q^2)$

$F_a(t) =$

Fitting F
the quadru
process. Fr
with the va
of strain.

The resu
are shown
[eq. (70)]:

$\langle\omega_Q^2\rangle$

where A is
tion densi

-42-

$\omega_1^2 \gg 1$

$$\frac{1}{T_{1\rho}}\Big|_D = \frac{\langle \omega_{ll}^2 \rangle \frac{\tau_m}{\tau_N}}{\omega^2 \tau_{NMR}} \Longleftrightarrow i = \phi\, b\, \rho_m \frac{L}{\tau_N}$$

$$\tau_{NMR} = \tau_N$$

$$\frac{1}{T_{1\rho}}\Big|_D = \frac{A_Q}{\omega_1^2 + \omega_{Loc}^2} \frac{i}{\phi b L}$$

PARAMETERS : A_Q , $\omega_{Loc}^2 = \omega_D^2 + \omega_Q^2$

- A_Q : Experimental — Line broadening : ρ_T; F.I.D. : ω_Q^2; $\omega_Q^2 = A_Q \rho_T$

- ω_{Loc}^2 : Experimental
  · Intersection of $(T_{1\rho})_D$ vs H_1^2 with H_1^2 axis:

$$(T_{1\rho})_D = 0 = \frac{\omega_1^2 + \omega_{Loc}^2}{A_Q^2} \phi b L$$

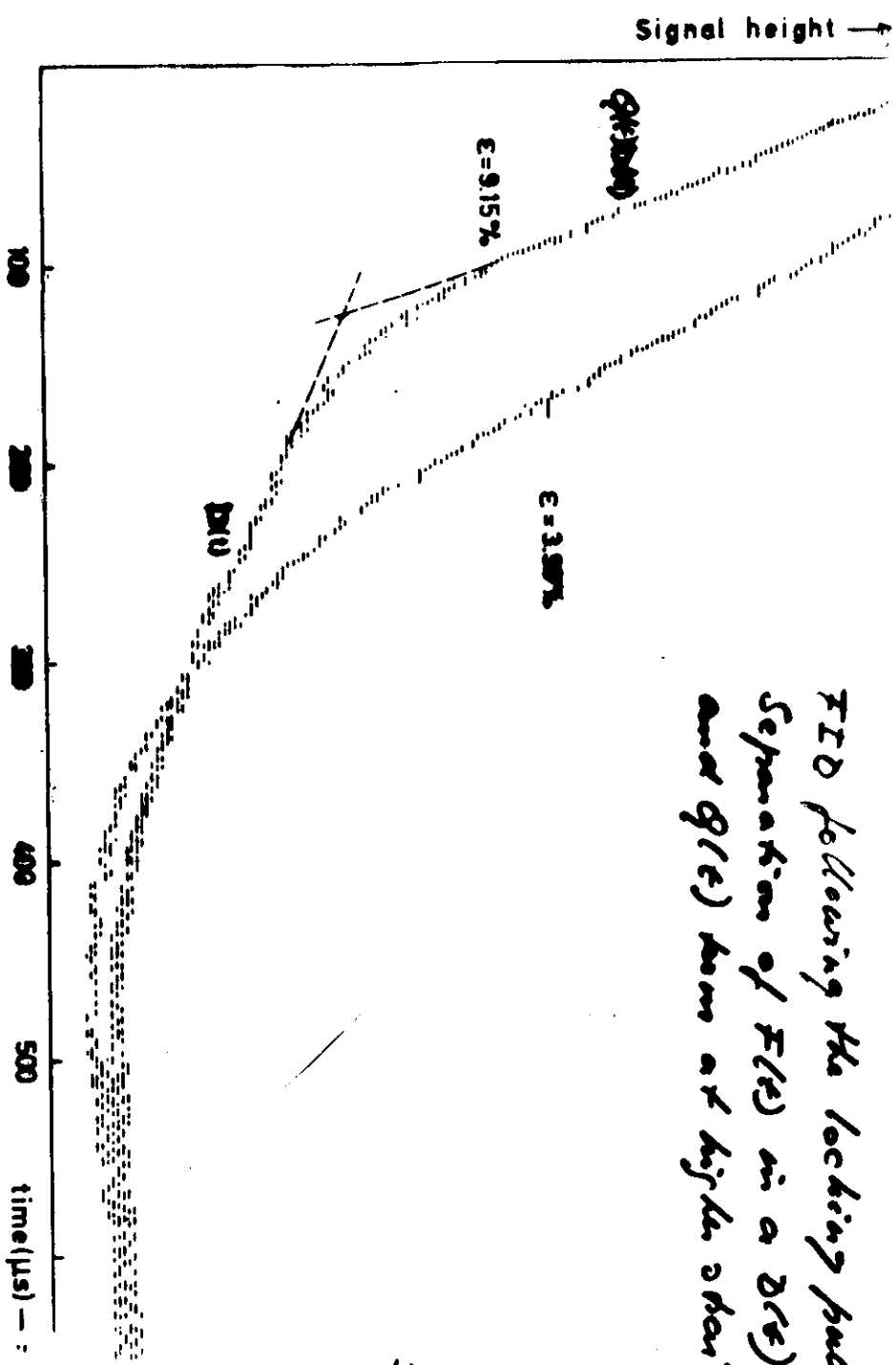

FID following the locking pulse
Separation of F(t) in a D(t)
and Q(t) term at high ε ratio

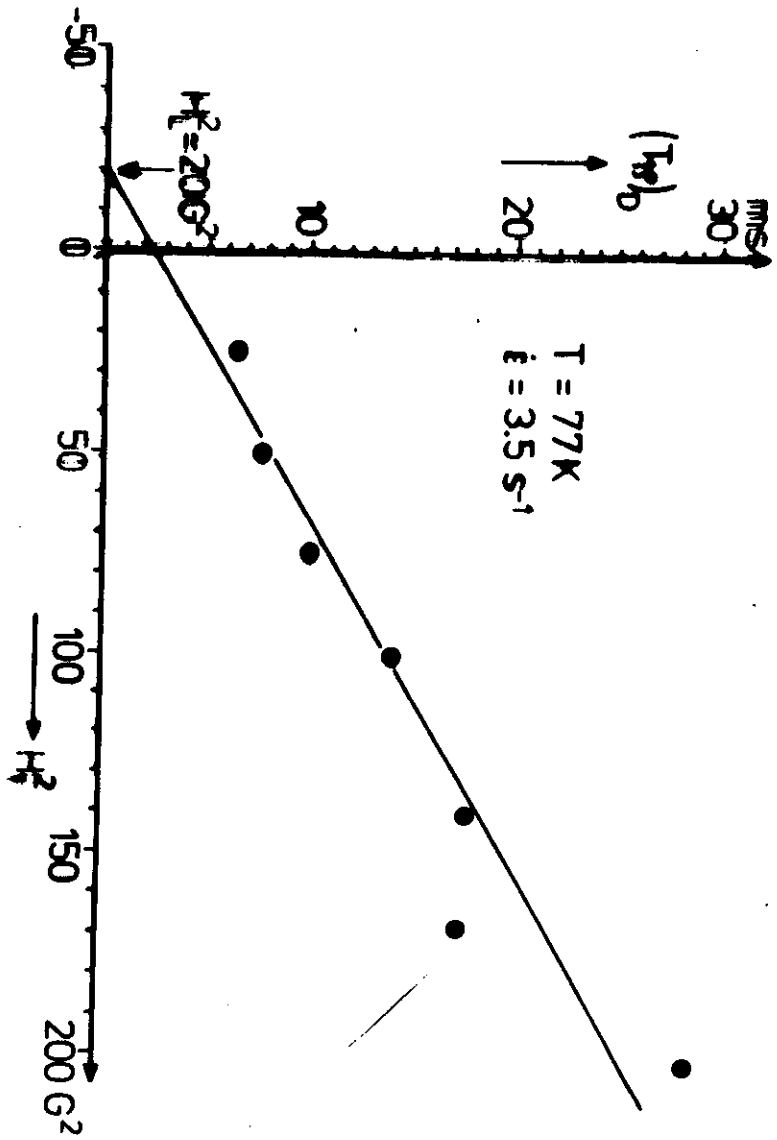

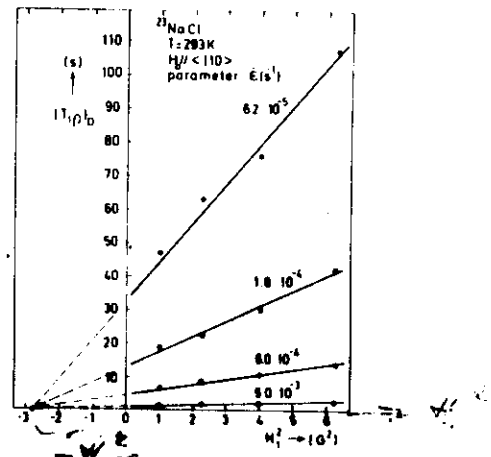

Fig. 32. $T_{1\rho D}$ of ^{23}Na versus H_1^2. The intersections of the lines with the abscissa are approximately at one point, given by $-2.6\,G^2$ [84, 145, 160].

Assuming Gaussian distribution functions [eqs. (55), (56) and (59)],

$$D(t) = \exp(-\tfrac{1}{2}\langle\Delta^2\rangle t^2), \tag{133}$$

and

$$Q(t) = \exp(-\tfrac{1}{2}\langle a^2\rangle t^2), \tag{134}$$

where $\langle\Delta^2\rangle^{1/2}$ and $\langle a^2\rangle^{1/2}$ are the dipolar and quadrupolar line widths ($\frac{1}{2}\langle\omega_D^2\rangle^{1/2}$ and $\frac{1}{2}\langle\omega_Q^2\rangle^{1/2}$, respectively), the resulting expression for $F_a(t)$ becomes:

$$F_a(t) = 0.4\exp(-\tfrac{1}{2}\langle\Delta^2\rangle t^2) + 0.6\exp(-\tfrac{1}{2}\langle\Delta^2\rangle t^2)\exp(-2\langle a^2\rangle t^2). \tag{135}$$

Fitting F_a to the measured free induction decay, the dipolar energy term $\langle\omega_D^2\rangle$ and the quadrupolar energy term $\langle\omega_Q^2\rangle$ can be obtained at several stages of the deformation process. From these analyses it was found that $\langle\omega_D^2\rangle \simeq 32\times10^6\ \mathrm{s}^{-2}$, in good agreement with the value $40\times10^6\ \mathrm{s}^{-2}$ as given by Hebel [164], and to first order independent of strain.

The results of the values for $\langle\omega_Q^2\rangle$ thus obtained as functions of the applied stress are shown in fig. 33. Using a statistical distribution of dislocations one may write [eq. (70)]:

$$\langle\omega_Q^2\rangle = A\rho = \gamma^2\delta_Q\langle V^2\rangle\rho, \tag{136}$$

where A is a constant ($\simeq 0.13\ \mathrm{cm}^2\ \mathrm{s}^{-2}$ for ^{23}NaCl) and ρ stands for the total dislocation density. Because of the linear relationship between $\langle\omega_Q^2\rangle^{1/2}$ and the applied

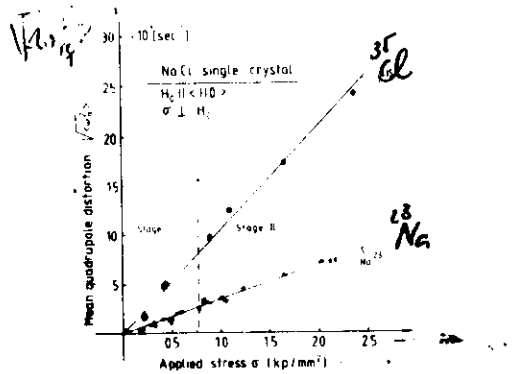

Fig. 33. Linear relationship for NaCl between the applied stress and $\langle\omega_Q\rangle^{1/2}$ measured on ^{23}Na and on ^{35}Cl. The different sensitivity of the two probes is mainly caused by the difference in the nuclear quadrupolar moments Q and in the gradient elastic constants (table 2) [84].

stress σ depicted in fig. 33, it confirms the well-known proportionality between the shear stress and $\rho^{1/2}$ in stage I and stage II which was found by Matucha et al. [52] and Hesse and Hobbs [34]. The maximum value of H_0^2 in these experiments was 1.3 G^2, which satisfies the condition that H_0^2 is not much larger than $H_{0t}^2 \simeq 0.6$ G^2).

Further evaluating eq. (129) quantitatively, a preliminary estimate of the average distance between obstacles encountered by a "jumping" dislocation can be made. Taking the curves for ^{23}NaCl in fig. 31 it is observed that

$$R\beta = C(H_1)H_1^2. \tag{137}$$

Numerical evaluation of the experimental results yields the value 161 for $C(H_1)$ at $H_1 = 2$ G. Quantitative agreement between eq. (129) and the experimental result [eq. (137)] is obtained, using eq. (136), only if

$$\frac{g_Q}{L} = C(H_1)\frac{\gamma^2 H_1^2 + \langle\omega_0^2\rangle + \langle\omega_Q^2\rangle}{A}\phi b, \tag{138}$$

where $\langle\omega_0^2\rangle + \langle\omega_Q^2\rangle = \gamma^2 H_L^2$. Inserting the values of $C(H_1)$, $\langle\omega_0^2\rangle \simeq 32 \times 10^6$ s^{-2}, $\langle\omega_Q^2\rangle = 16 \times 10^6$ s^{-2} (fig. 33), $\gamma^2 = 50 \times 10^6$ G^{-2} s^{-2}, $A = 0.13$ cm^2 s^{-2}, $\phi = 0.5$ and $b = 0.396$ nm, it follows that:

$$\frac{g_Q}{L} \simeq 6.31 \times 10^5 \text{ m}^{-1}. \tag{139}$$

From the calculated values of g_Q/Nb (sect. 4) it is concluded that only dislocation jumps across large distances satisfy this equality. Taking g_Q approximately equal to 1, L is equal to about 4000 Burgers vectors ($\simeq 1.6 \times 10^{-6}$ m). This value found for L

obstacles are referred to as "strong" obstacles. In alkali halide crystals of monovalent ions, divalent impurities are effective obstacles. To preserve charge neutrality in the lattice, each impurity ion, e.g. a Ca^{2+} ion in NaCl, is associated with a cation vacancy. These dipoles interact with dislocations and therefore also influence the mechanical properties. At temperatures below 150 C the obstacles are fixed and can be overcome only by thermal activation, whereas at higher temperatures the defects become mobile and are able to follow the moving dislocations, which gives rise to a drag force. Apart from single dipoles, aggregates of dipoles are also present in the crystal. Their number and distribution depend strongly on the thermal treatment previous to the deformation and on the temperature of deformation itself [169].

Considering the fact that the mean free path L in eq. (129) is determined by the mean distance d_t between forest dislocations and by d_p, the mean distance between point defects, eq. (129) is refined by insertion of:

$$\frac{1}{L} = \frac{1}{d_t} + \frac{1}{d_p}. \tag{142}$$

Relaxation measurements have been performed on NaCl (001) single crystals doped with different amounts of $CaCl_2$ ranging from 7 to 340 mol ppm in the temperature range from 10–270 C. The spin–lattice relaxation rate in the rotating frame is measured by means of the spin-locking technique. In fig. 36 the value of $R\beta = T_{1\rho}^{-1}(\dot{\varepsilon} \neq 0)$ is depicted as a function of the strain rate $\dot{\varepsilon}$ in the direction of the compression axis for single crystals doped with different amounts of impurities. Raising the concentration of impurities will diminish the mean distance d_p and therefore the relaxation rate will increase. The mean free path L can be determined with the aid of eq. (129), yielding for pure crystals a value for d_t of about 1.0 μm. Evaluation of the data using eq. (142) gives values for d_p which are plotted in fig. 37. These results do not correspond with the values obtained from calculations of the mean distance between

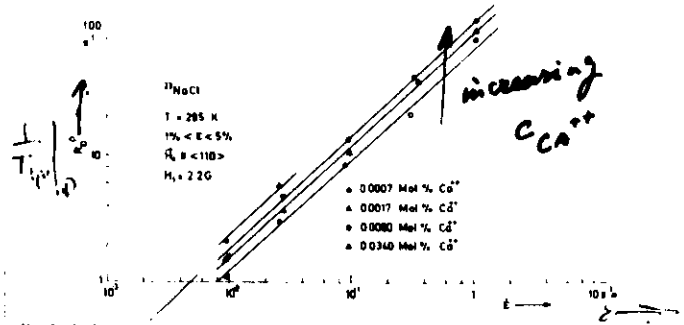

Fig. 36. Dislocation-induced part of the relaxation rate $R\beta$ as a function of the strain rate $\dot{\varepsilon}$ in ^{23}NaCl single crystals doped with different amounts of impurities [170].

function of temperature in ^{23}NaCl

l as functions of temperature.
ure single crystals (impurity
and 690 mol ppm Ca^{2+} ions.
$/T_{1\rho}$ in the undoped crystals
exponential increase occurs
s found from the slope of the
is region the cation-vacancy
gy corresponds to the above-
f the cation vacancy has been
e ionic conductivity of doped
ever, a certain discrepancy in
.72 eV [175] to 0.85 eV [176].
he *static* relaxation rate $T_{1\rho}^{-1}$
. The as-grown crystals show
the crystals after an anneal at
have higher rates increasing

with a slope of 0.31 eV. These values are close to the dissociation energy of dimers (a configuration of two dipoles). Crawford [177] presented a corpus of ideas regarding the processes underlying the aggregation of divalent cation impurity dipoles. It was shown that the third-order kinetics experimentally observed by Dryden [178] which governs the aggregation can be accounted for on the basis of a two-step process, namely: (a) two dipoles come together to form a loosely coupled pair which in turn (b) captures a third dipole to form a trimer. This process can yield a reaction rate proportional to the third power of the dipole concentration only if the dimers are in quasi-equilibrium with the free dipoles, a condition which implies that the energy binding the pair is rather small ($\gtrsim 0.2$ eV). Nevertheless, the activation energy for the segregation reaction in NaCl:Ca^{2+} is rather small (0.04 eV) which is probably too small to be significant. Dubiel et al. [179] concluded from T_1 spin-lattice relaxation time measurements in NaCl:Ca^{2+} that aggregation processes take place in the range up to 200°C. For higher temperatures no change in the dipole concentration could be measured. For doping up to 500 ppm mainly dimers and trimers were formed. Analysing their experimental curves they concluded that the enthalpy for the dipole motion was about 0.6 eV and the dimer association enthalpy about equal to 0.3 eV, which is in accordance with the results presented in fig. 39.

Measurements of $T_{1\rho}$ on deforming crystals as a function of temperature yielded the data depicted in fig. 40. They were obtained at a strain rate $\dot{\varepsilon} = 0.4\ s^{-1}$ with deformations of $\varepsilon = 3\%$ and 7% for the undoped crystals and about 5% for the doped crystals. It can be seen that the room-temperature value of the mean free path for moving dislocations hardly changes in the region up to 150°C. The very few impurities are fixed obstacles with respect to the mobile dislocations and the interactions of the moving dislocations with forest dislocations dominate the magnitude of L. Therefore

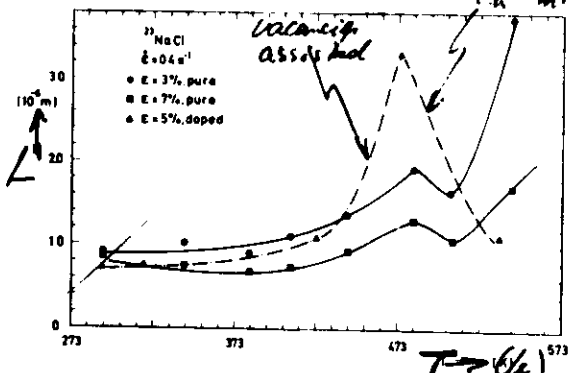

Fig. 40. The mean free path L as a function of temperature for pure and for doped (40 mol ppm Ca^{2+}) NaCl (100) crystals using a strain rate $\dot{\varepsilon} = 0.4\ s^{-1}$ [170].

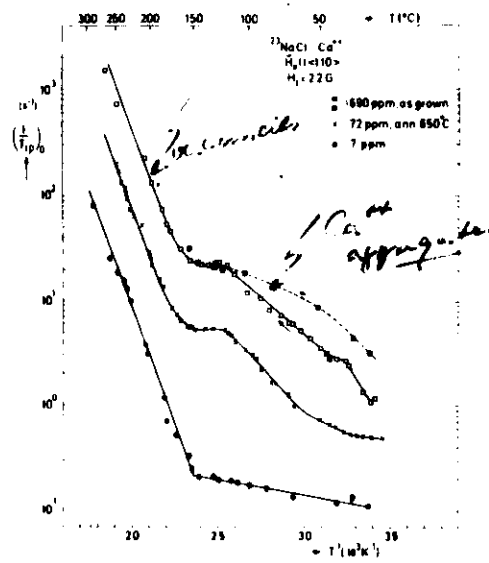

Fig. 39. The static spin-lattice relaxation rate in the rotating frame as a function of temperature in ^{23}NaCl ($\dot{\varepsilon} = 0$) [107, 172].

In fig. 39 spin-lattice relaxation rates $T_{1\rho}^{-1}$ are depicted as functions of temperature. These static measurements were performed on ultra-pure single crystals (impurity concentration $\ll 10$ ppm) and on crystals containing 72 and 690 mol ppm Ca^{2+} ions. Up to temperatures of about 150°C the lattice part of $1/T_{1\rho}$ in the undoped crystals increases with T, whereas above this temperature an exponential increase occurs with an activation energy of 0.89 eV. The same energy is found from the slope of the high-temperature part of $T_{1\rho}^{-1}$ in doped crystals. In this region the cation vacancy diffusion is the dominant process and the migration energy corresponds to the above-mentioned value [174]. The effective activation energy of the cation vacancy has been determined by Dreyfus and Nowick [174] based on the ionic conductivity of doped NaCl crystals, and was found to be about 0.8 eV. However, a certain discrepancy in this value exists among various authors, ranging from 0.72 eV [175] to 0.85 eV [176].

In the temperature range between 50°C and 180°C the *static* relaxation rate $T_{1\rho}^{-1}$ depends on the thermal treatment of the doped crystals. The as-grown crystals show an exponential increase with a slope of 0.36 eV, while the crystals after an anneal at 650°C and cooling to room temperature at 50°C/min have higher rates increasing

with a slope of 0.31 eV. Tl
configuration of two dipo
the processes underlying
shown that the third-orde
governs the aggregation
namely: (a) two dipoles co
captures a third dipole to
portional to the third po
quasi-equilibrium with th
binding the pair is rather
segregation reaction in N
small to be significant. D
time measurements in Na
up to 200°C. For higher t
measured. For doping
Analysing their experime
motion was about 0.6 eV
which is in accordance w

Measurements of $T_{1\rho}$
the data depicted in fig. 4
mations of $\varepsilon = 3\%$ and 7%
tals. It can be seen that th
dislocations hardly chan
fixed obstacles with resp
moving dislocations with

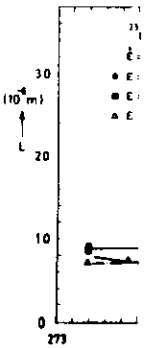

Fig. 40. The mean free path L
NaCl

MEAN TIME OF STAY τ_w

MOBILE DISLOCATION DENSITY ρ_m

General equation:

$$\left(\frac{1}{T_{1\rho}}\right)_D = C(H_1)\,\frac{\rho_m}{\rho_t}\,\frac{\omega_{eff}\,\tau_w}{1+4\,\omega_{eff}^2\,\tau_w^2}$$

$$\omega_{eff}^2 = \omega_1^2 + \omega_{loc}^2$$

At maximum:

$$4\,\omega_{eff}^2\,\tau_w^2 = 1 \longrightarrow \underline{\tau_w = \frac{1}{2\,\omega_{eff}}}$$

$$\longrightarrow \underline{\rho_m = \frac{2\,\tau_w}{\phi\,b^2}}$$

$$T_{1\rho}^{-1}\Big|_{max} = \frac{1}{4}\,C(H_1)\,\frac{\rho_m}{\rho_t} \longrightarrow \underline{\frac{\rho_m}{\rho_t}}$$

$$R_D^{(\rho)} = F\,\frac{\omega_1^2\,\tau_w}{1+4\,\omega_{eff}^2\,\tau_w^2}$$

EXPERIMENTS: "METALLIC MATERIALS"

TENSILE:

- ^{27}Al
- ^{27}Al - (0.1 - 10 at% Cu)
- ^{27}Al - 10 at% Li
- ^{27}Al - (1 - 2 at% Zn)
- ^{27}Al - 1 at% Mg
- ^{27}Al - Mg - Zn?

FATIQUE:

- ^{27}Al
- ^{27}Al - 0.5 at% Cu - 8 at% Li

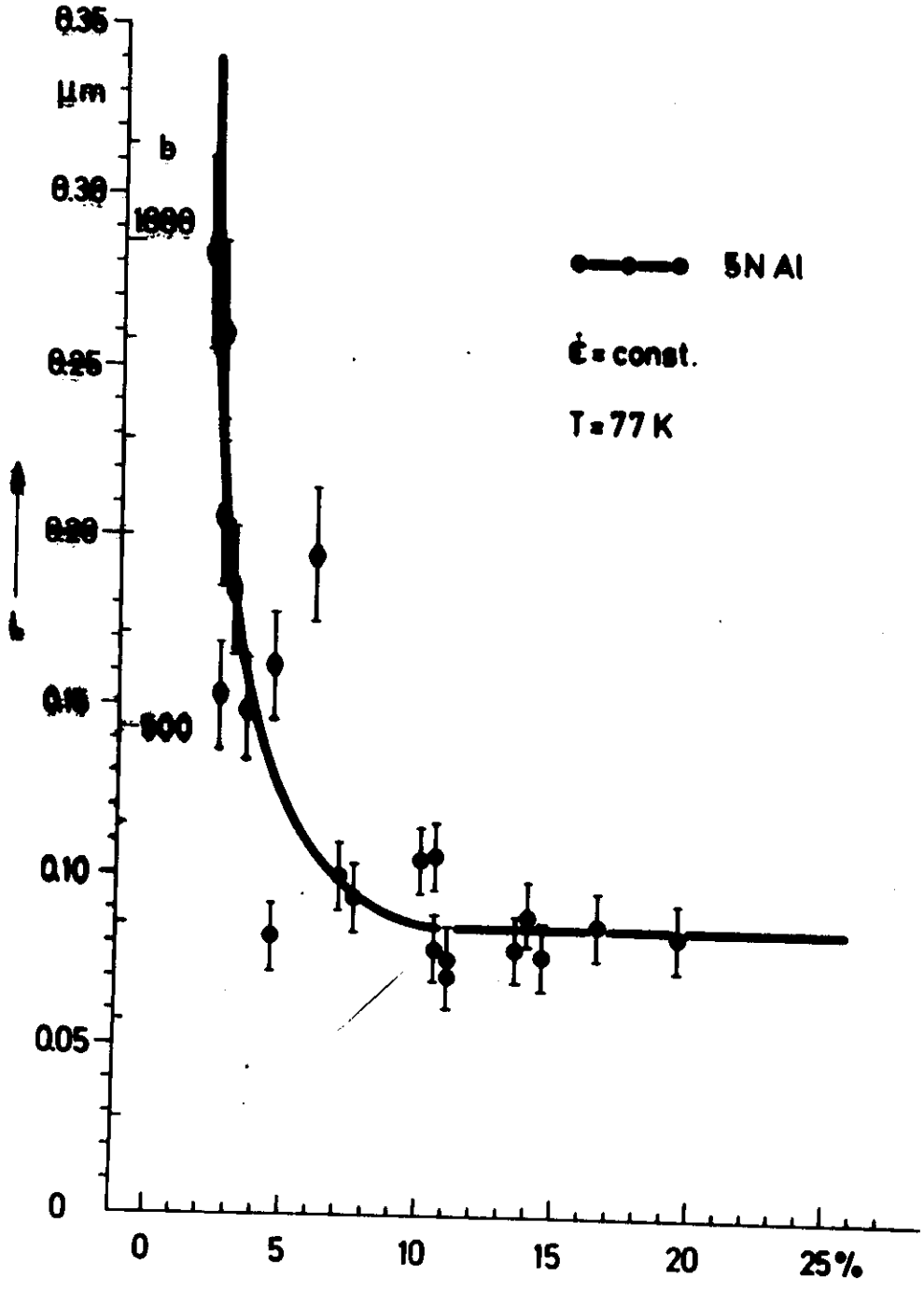

slip length Λ_s ≠ jump distance !

All moving dislocations present both in the cell wall (ρ_2) and in the interior region (ρ_1) without (τ_{IP}^{-1})$_D$

$L_1 \cong \Lambda_s$ (cell diameter ≅ 1 μm)

L_2 ≅ spacing of tangles ≅ 0.01 - 0.1 μm

$$\frac{1}{\tau_{IP}}\int_D^{tot} = \frac{1}{\tau_{IP}}\int_D^{(1)} + \frac{1}{\tau_{IP}}\int_D^{(2)}$$

$$\frac{1}{\tau_{IP}}\int_D^{(1)} \approx \frac{1}{L_1} \qquad \frac{1}{\tau_{IP}}\int_D^{(2)} \approx \frac{1}{L_2}$$

$$\boxed{\frac{1}{\tau_{IP}}\int_D^{tot} \approx \frac{1}{\tau_{IP}}\int_D^{(2)}}$$

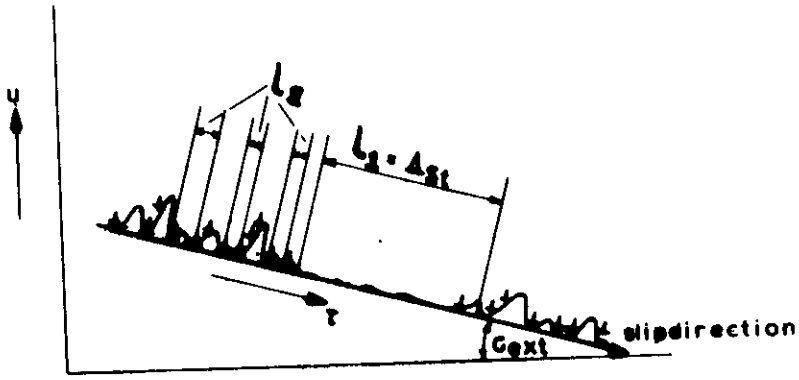

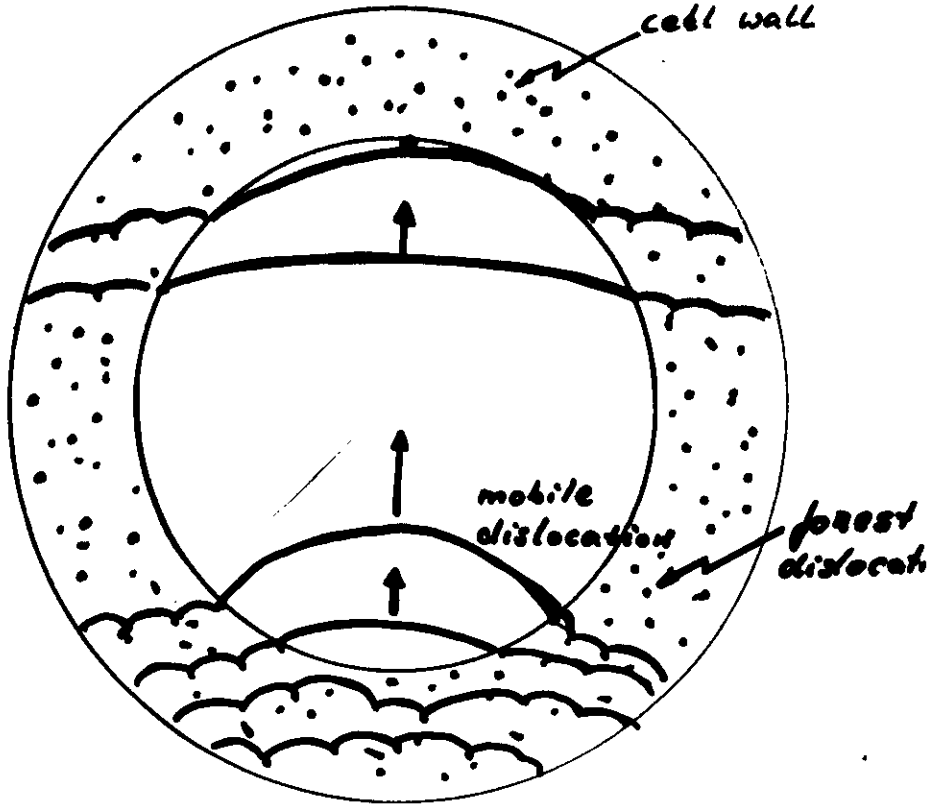

Al-Cu alloys

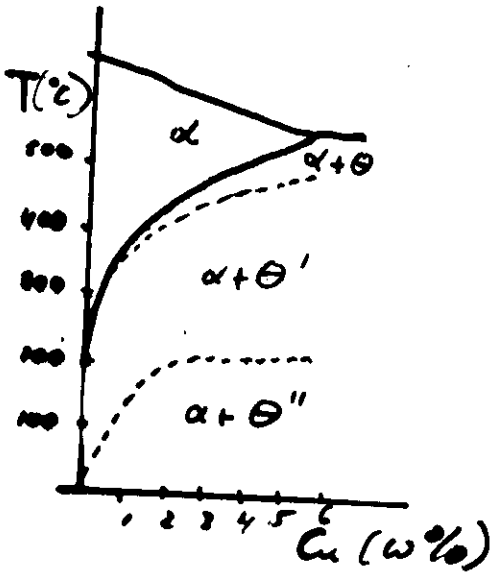

Θ'

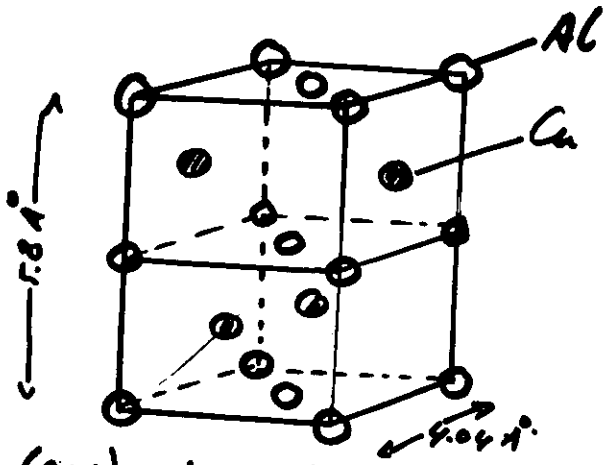

(001) coherent

(010) } Semicoherent
(100) } (interfacial dislocations)

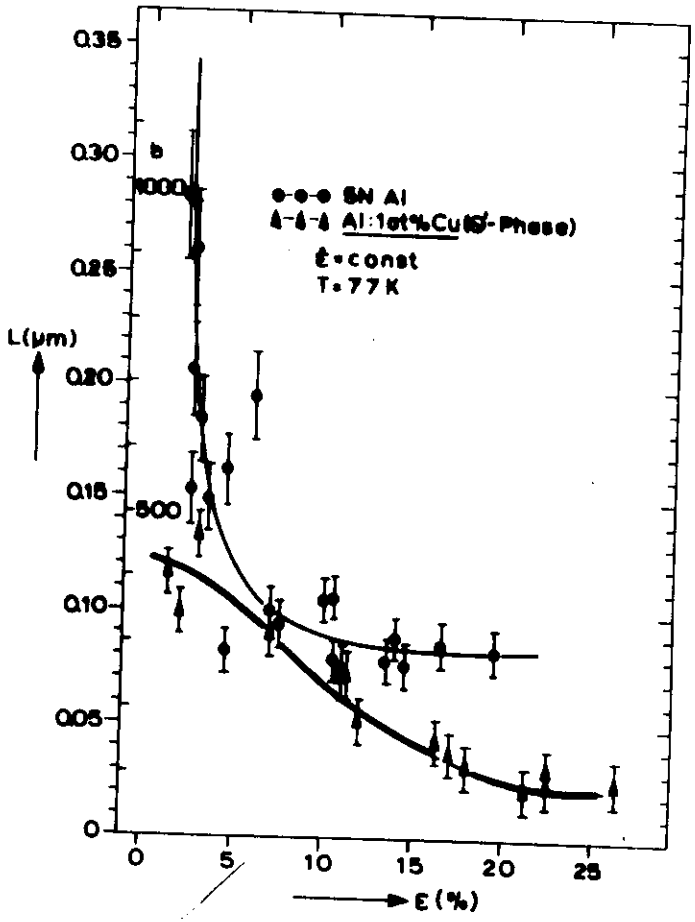

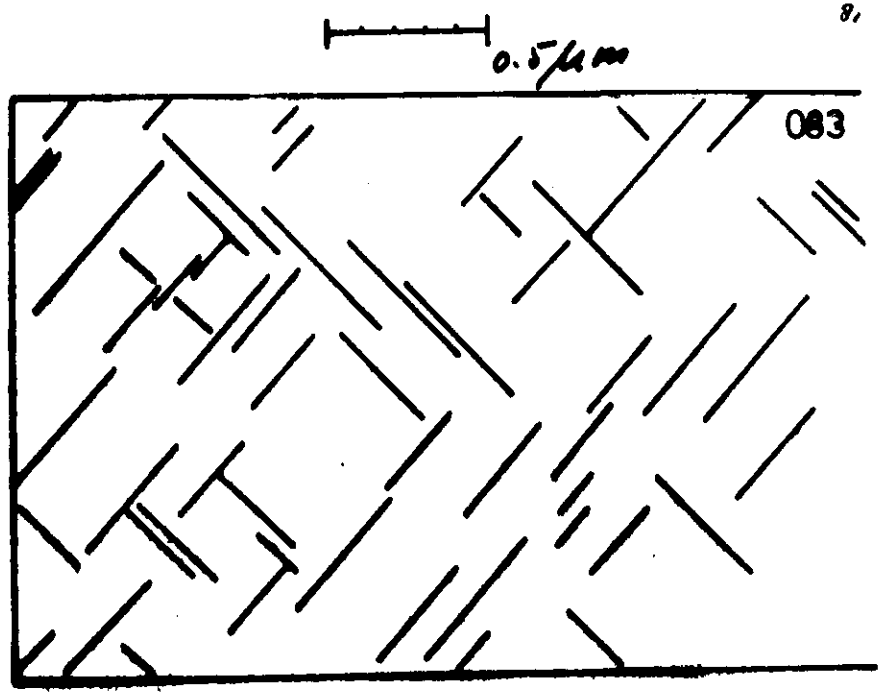
0.5 µm
083

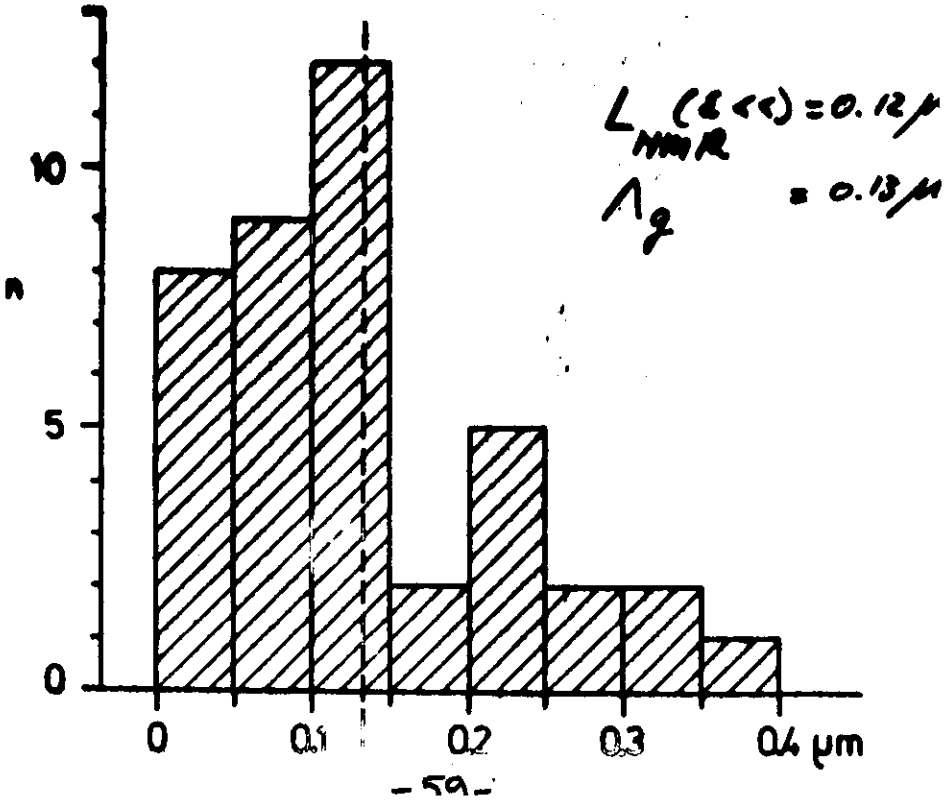
$L_{NMR}(\xi<<) = 0.12\,\mu$
$\Lambda_g = 0.13\,\mu$
n
10
5
0
0
0.1
0.2
0.3
0.4 µm

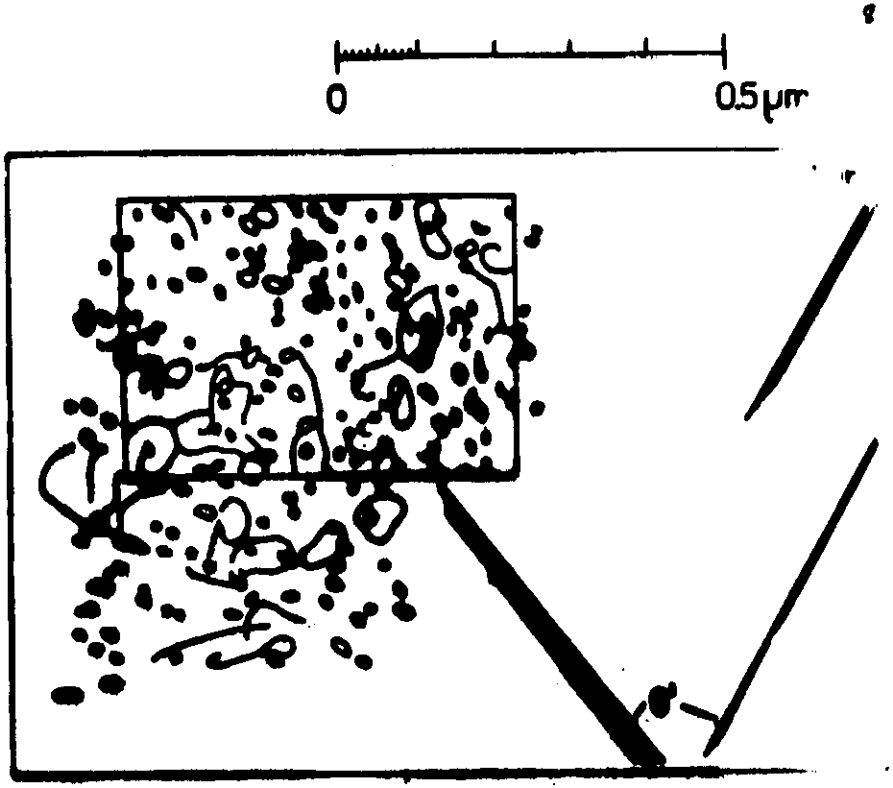
0
0.5µm

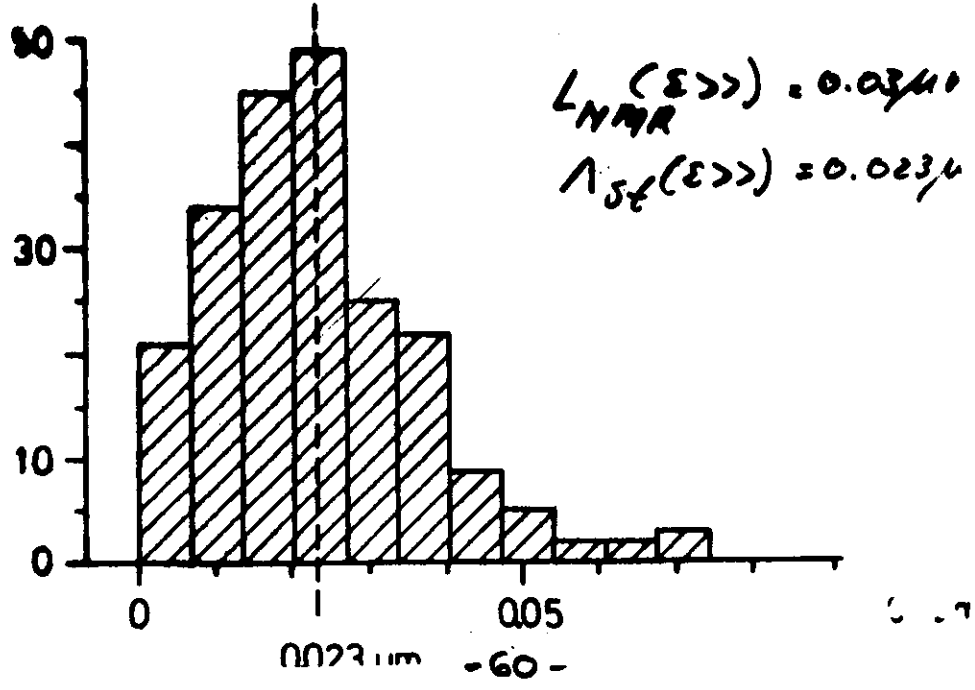
$L_{NMR}(\xi>>) = 0.03\,\mu$
$\Lambda_{sc}(\xi>>) = 0.023\,\mu$
n
50
30
10
0
0
0.05
0.023 µm

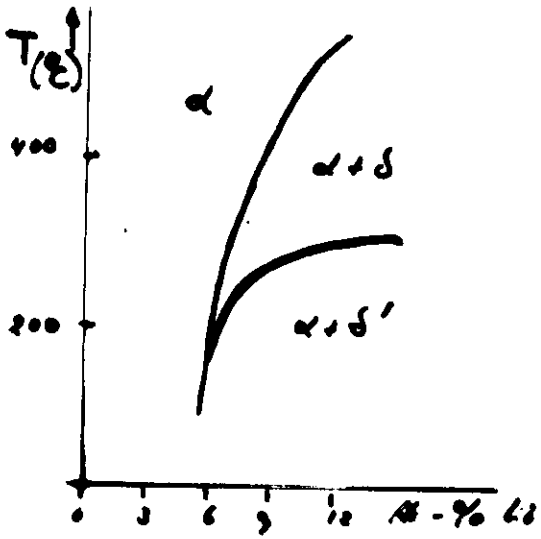

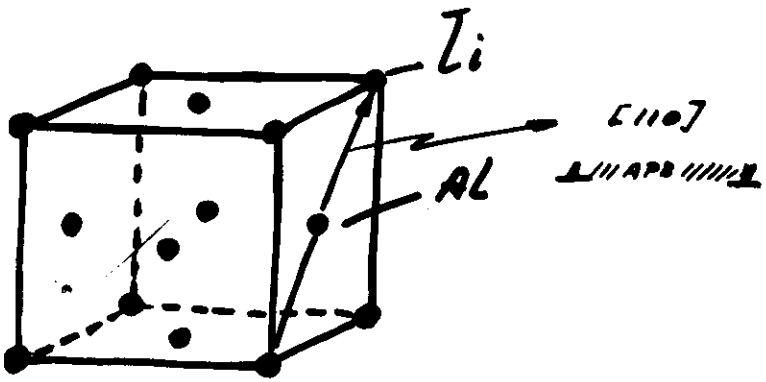

δ': Al_3Li

coherent (very small misfit strain)

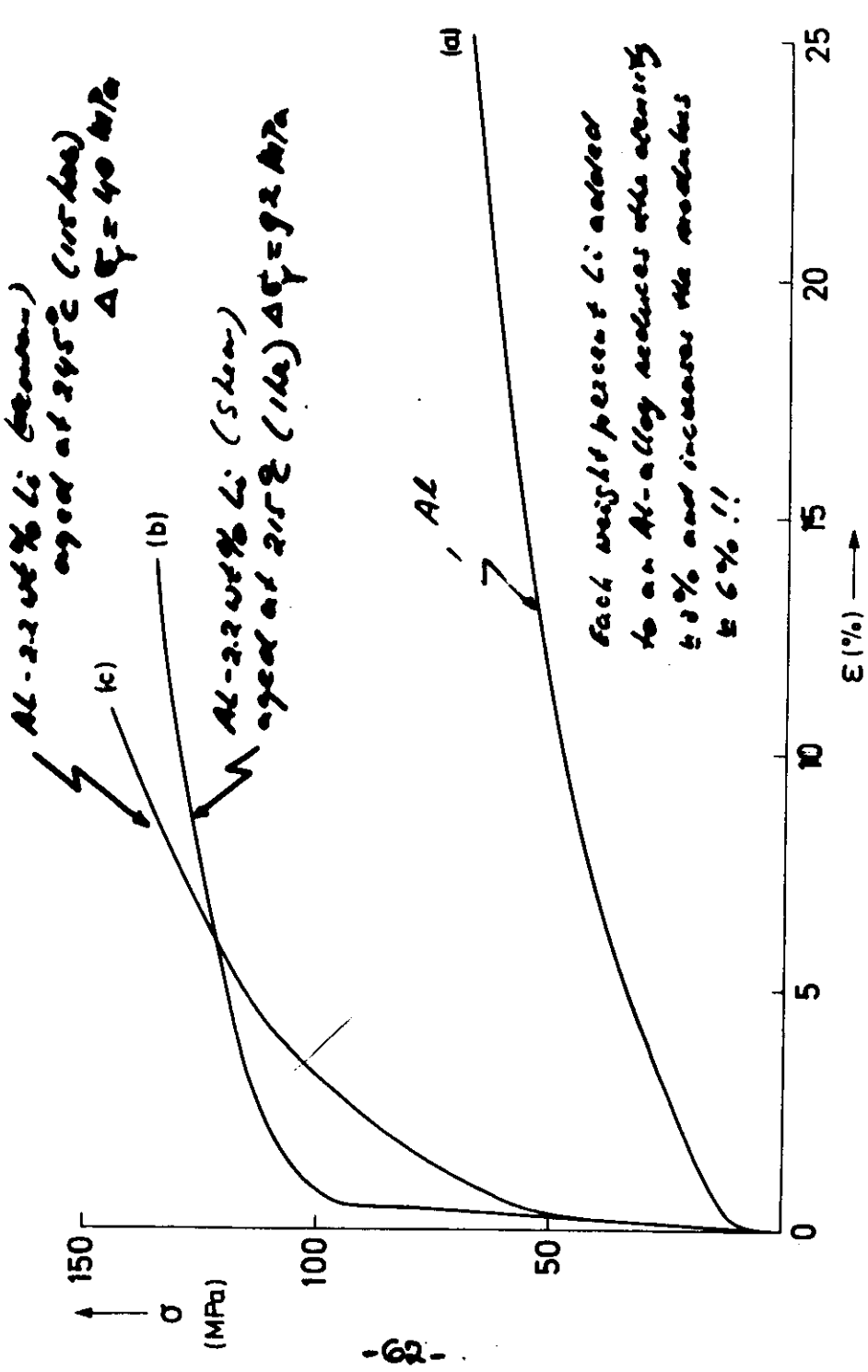

POSSIBILITIES

(1) SHEARING

(2) LOOPING

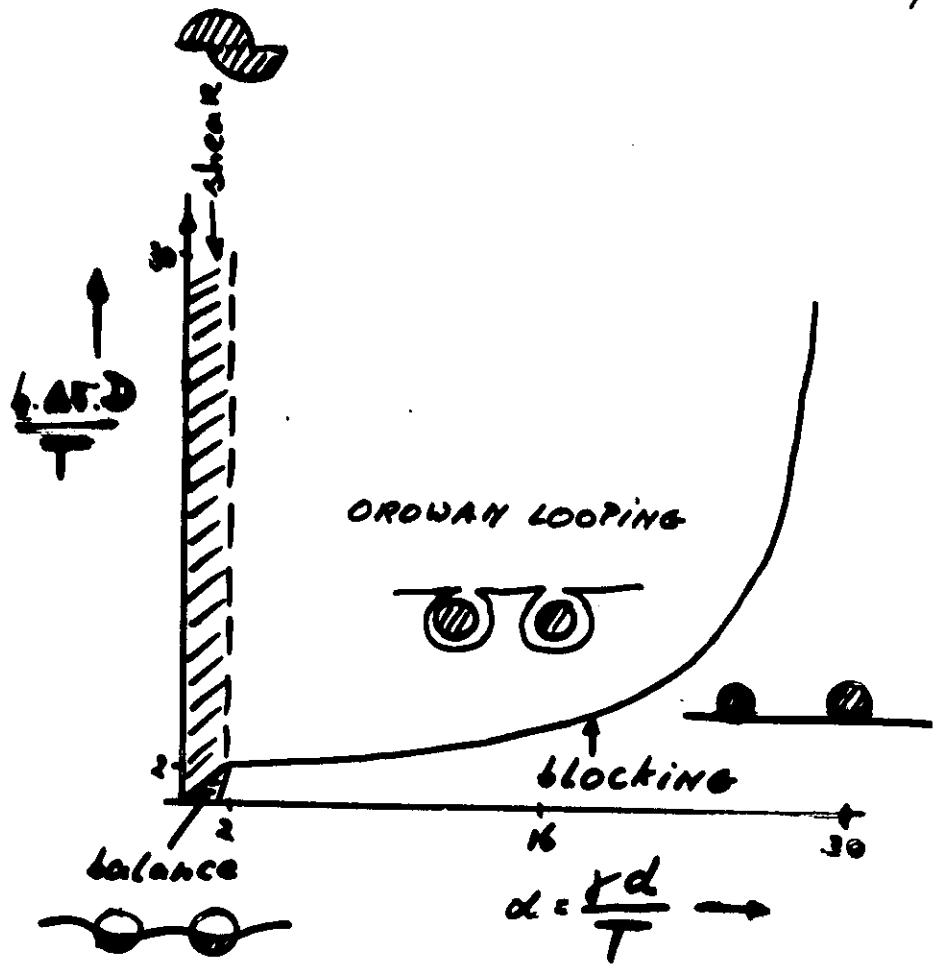

	EXP.	SHEAR
Al-Li 215°C 16h	$\Delta\sigma$ = 92 MPa	$\Delta\sigma_{calc}$ = 94.1 Mi
		OROWAN
Al-Li 245°C 115hrs	$\Delta\sigma$ = 40 MPa L_{NMR} = 0.25μm	$\Delta\sigma_{calc}$ = 45.9 MP

Al_3Li

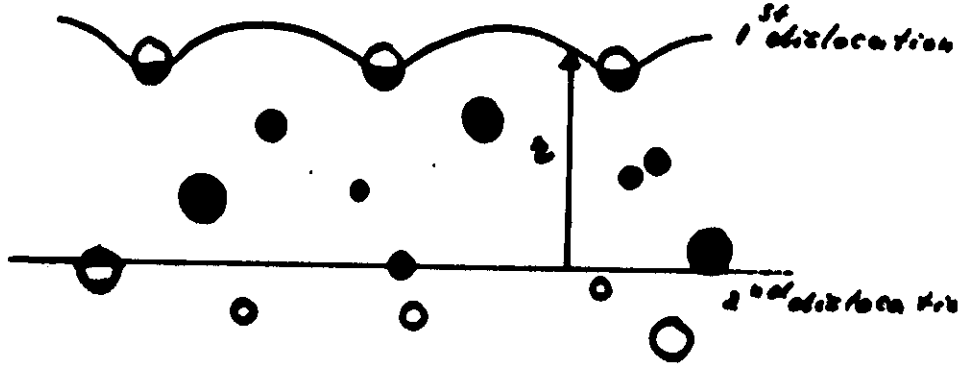

red-coloured areas show the existence of Antiphase boundaries within precipitates

calculated $E^{APB} = \frac{-2\omega}{a^2\sqrt{3}}$ → 123 mJ/m²

observed $E^{APB} = \frac{\mu b^2}{2\pi 2 f}$ → 185 mJ/m²

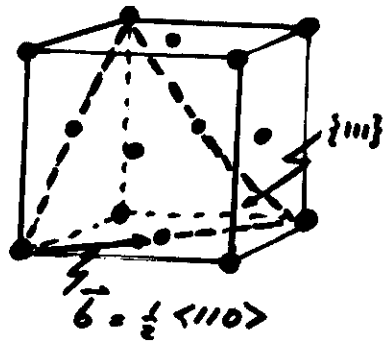

ACTIVATION LENGTH: d $\quad \dot{\varepsilon} = \dot{\varepsilon}_0 e^{-\Delta G/kT}$ (62)

$$V = -\left(\frac{\partial \Delta G}{\partial \tau}\right)_T = kT\left(\frac{\partial \ln \dot{\varepsilon}}{\partial \tau}\right)_T \propto d\, b^2$$

MEAN JUMP DISTANCE $\Longleftrightarrow$ MEAN ACTIVATION LENGTH

L_{NMR} $\qquad$ d

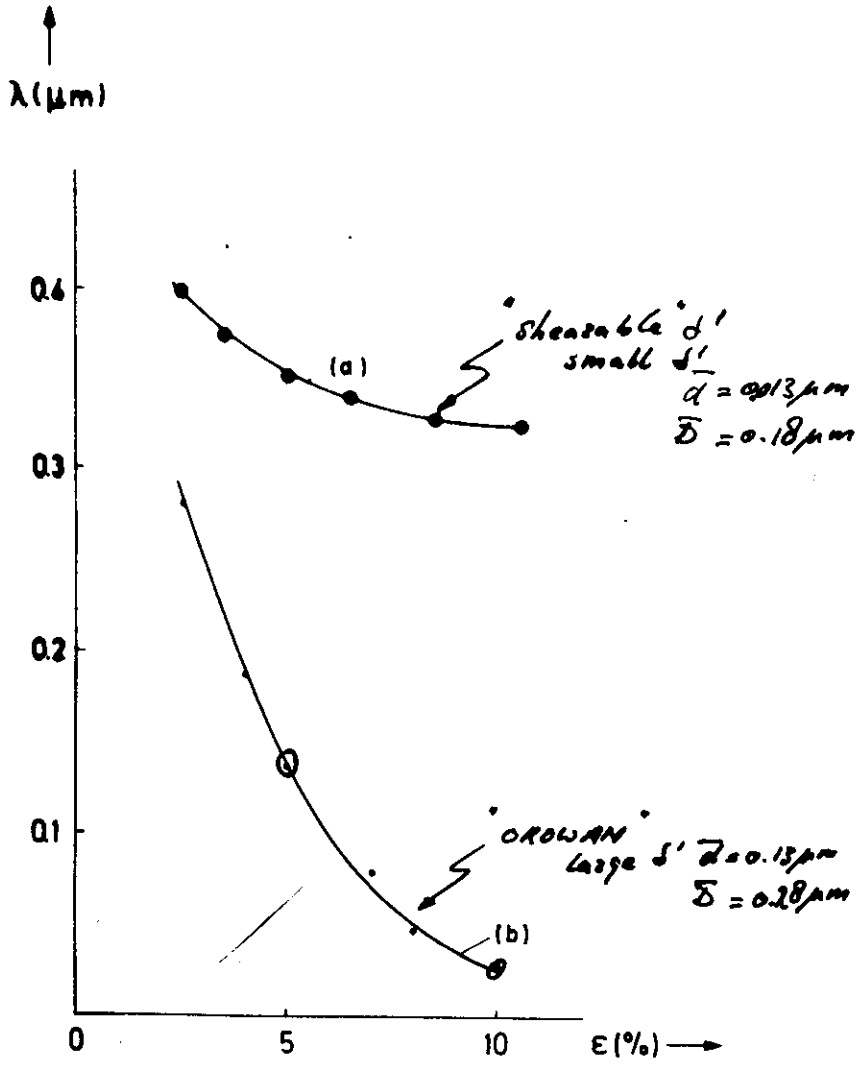

NON-SHEARABLE PRECIPITATES:

$$\left(\frac{1}{\tau_{IC}}\right)_{NS} = \left(\frac{1}{\tau_{IC}}\right)^{(1)}_{FOREST} + \left(\frac{1}{\tau_{IC}}\right)^{(2)}_{\text{NON-SHEARABLE PRECIPITATES}}$$

$$\frac{1}{L_{NMR}} \propto \frac{\rho_1}{d\,\rho_m} + \frac{\rho_2}{L_p\,\rho_m}$$

$d(\varepsilon = 5\%) = 0.19\,\mu m$, $L_p = 0.3\,\mu m$ $\longrightarrow$ $L_{NMR} = 0.19\,\mu m$ (measured $0.2\,\mu$)

$d(\varepsilon = 10\%) = 0.04\,\mu m$ $\longrightarrow$ $L_{NMR} = 0.07\,\mu m$ ($0.08\,\mu$)

SHEARABLE PRECIPITATES:

$L_p = f(\varepsilon)$ (?)

$\bar{d} = f(\varepsilon)$ (?)

$$\frac{1}{L_{NMR}} = \frac{\rho_1}{d\,\rho_m} + \frac{\rho_2}{L_p\,\rho_m} + \frac{\rho_3}{\bar{d}\,\rho_m}$$

SOLID SOLUTION

Al - Zn (0.5 - 2 at%)

FRIEDEL's MODEL
no internal stress

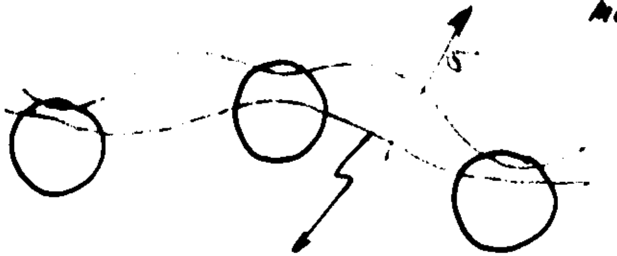

MOTT-NABARRO's MODEL

due to internal stress

$\tau_i \approx \mu |\delta| c \ln 1/c$

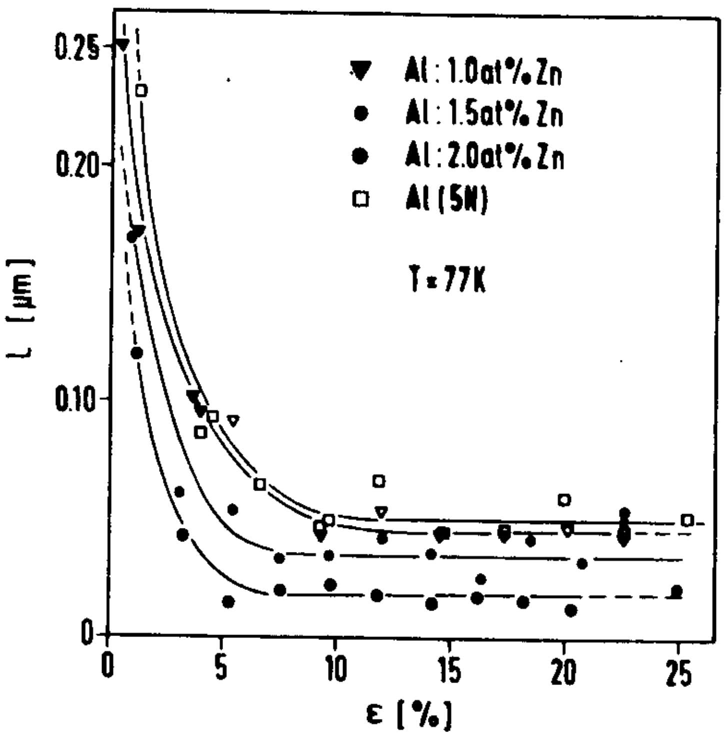

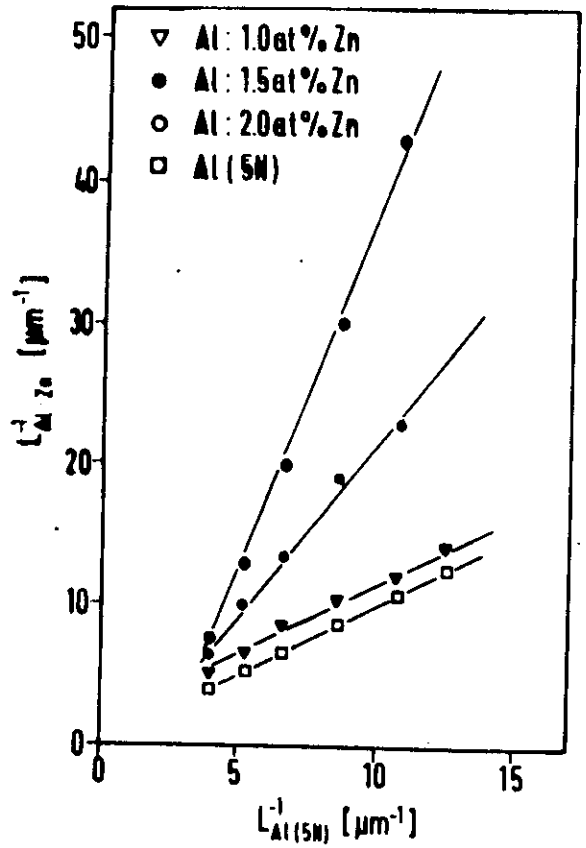
Al : 1.0at% Zn
Al : 1.5at% Zn
Al : 2.0at% Zn
Al (5N)
50
40
30
20
10
0
0
5
10
15
$L^{-1}_{Al\ Zn}$ [μm^{-1}]
$L^{-1}_{Al\ (5N)}$ [μm^{-1}]

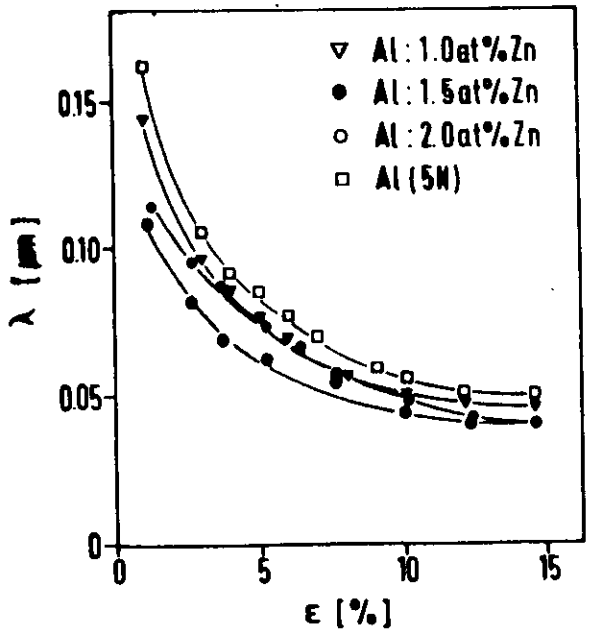
Al : 1.0at%Zn
Al : 1.5at%Zn
Al : 2.0at%Zn
Al (5N)
0.15
0.10
0.05
0
0
5
10
15
ε [%]

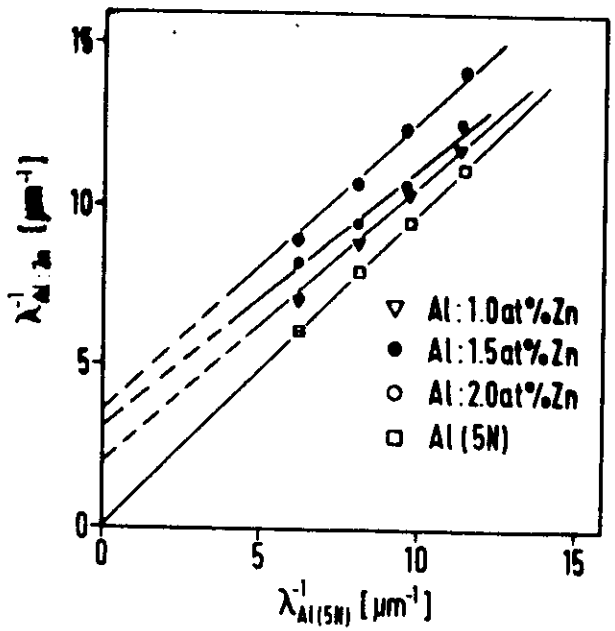

SOLUTE SPACING μm

	MIROSL	MOTT HABARRO	NMR	$\dot{\varepsilon}$ Cham
1% Zn	0.04	0.15	0.19	
1.5% Zn	0.03	0.11		
2% Zn	0.02	0.09		

NMR is a complementary (TEM!) new technique for the study of dislocations IN METALLIC AND IONIC CRYSTALS